RAMAN SPECTROSCOPY OF MOLECULES WITH INTERNAL DEGREES OF FREEDOM

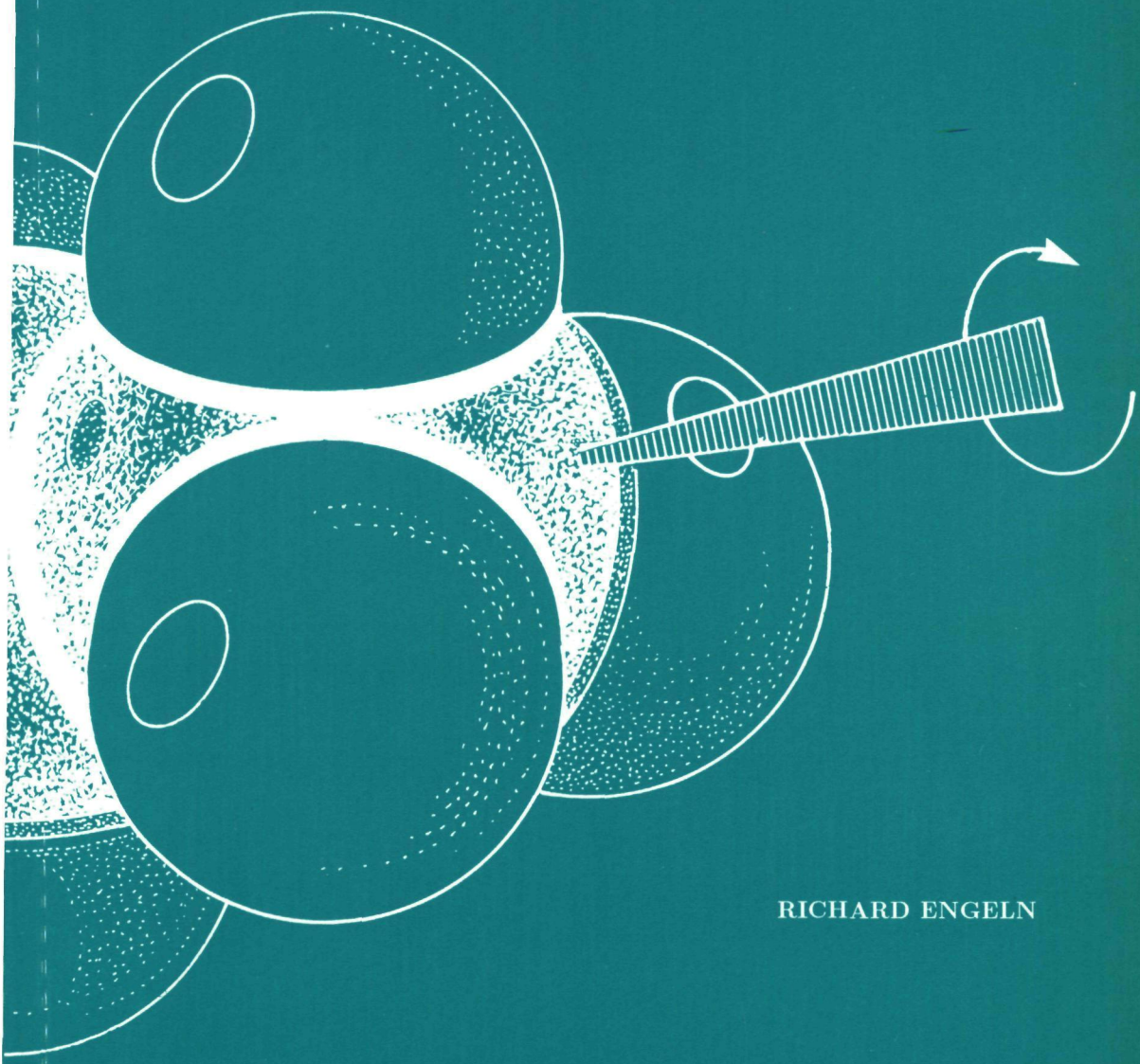

RICHARD ENGELN

RAMAN SPECTROSCOPY OF MOLECULES WITH INTERNAL DEGREES OF FREEDOM

RAMAN SPECTROSCOPY OF MOLECULES WITH INTERNAL DEGREES OF FREEDOM

EEN WETENSCHAPPELIJKE PROEVE OP HET GEBIED VAN
DE NATUURWETENSCHAPPEN

PROEFSCHRIFT

TER VERKRIJGING VAN DE GRAAD VAN DOCTOR
AAN DE KATHOLIEKE UNIVERSITEIT TE NIJMEGEN,
VOLGENS BESLUIT VAN HET COLLEGE VAN DECANEN
IN HET OPENBAAR TE VERDEDIGEN
OP DONDERDAG 3 OKTOBER 1991,
DES NAMIDDAGS TE 3.30 UUR

door

RICHARD ANTONIUS HENDRICUS ENGELN

geboren op 13 februari 1964
te Geleen

Promotor : Prof. Dr. J. Reuss

Dankwoord

Op deze plaats wil ik alle mensen bedanken, die op enigerlei wijze een bijdrage hebben geleverd aan het tot stand komen van dit proefschrift. Enkelen van hen wil ik met naam noemen:

- Freek, met wie ik samen met 'onze jongens', Madonna en de visjes drie jaar lang de kamer heb gedeeld.
- Mijn begeleider, J. Reuss, met zijn aanstekend enthousiasme en interesse voor het onderzoek. Daarnaast wil ik hem ook nog bedanken voor de mogelijkheden die hij mij in de afgelopen vier jaar heeft geboden om onderzoek te kunnen doen in het buitenland; een keer drie maanden en een keer een maand CARS in Frascatie. De tijd die ik daar heb doorgebracht is onvergetelijk gemaakt door Roberta en Susanna. Roberta heeft mij op ENEA alle vrijheden gegeven die je nodig hebt om in een (altijd 'te') korte tijd toch tot goede resultaten te komen. Susanna heeft mij samen met haar vrienden, een beetje de Italiaanse levenswijze bijgebracht.
- Nico die mij tijdens het afstuderen leerde wat experimentele natuurkunde inhoudt.
- Alle overige vaste medewerkers en AIO's die 'onze kant' en 'de andere kant' tot de afdeling Molecuul- en Laserfysica maken. Met name degenen die tijdens de lunchpauzes van de studentenkamer een echte koffiekamer maakten: Lukas, Sacco, Huug, Frans, Frans, Ger en Mark.
- Annet, wier hulp onontbeerlijk is.
- Cor, John, Frans en Eugène die een oplossing hebben voor ieder probleem en die het mogelijk maakten de opstelling vier jaar draaiende te houden. Cor wil ik nog bedanken voor de zeildagen waar hij voor mij 'Kaptein' Sikkens werd.
- Hans voor het ontwikkelen en tekenen van DE cel, Daniela voor de hulp bij veel van de experimenten die in dit proefschrift beschreven staan en John van de afdeling Theoretische Chemie, die mij met zijn computerprogramma's hielp menig 'two-top'-spectrum te analyseren.
- Jose-Maria Fernández-Sánchez die mij op het 'rotor-spoor' bracht.
- De medewerkers van de grote werkplaats, quick-service, glasblazerij, illustratie en fotografie, en uiteraard Ferry van de zelfservice. Hoewel de naam 'zelfservice' doet vermoeden dat je daar alles zelf moet doen, is het vaak Ferry-made.

Contents

Chapter 1

Preface

The results presented in this thesis are achieved using a Raman setup. A short historical overview of Raman spectroscopy is given and for a classical and quantum mechanical description of this light scattering phenomenon the textbook of D.A. Long [1] is recommended. The experimental setup, used to study internal motions in floppy molecules, is extensively described. One type of internal motion is the torsional motion.

The torsional potential of a CH_3-group in a molecule can be described approximately by $V_3 \cos 3\phi$, ϕ being the torsional angle. The potential parameter V_3 - and the reduced rotational constant of the top, F, as it occurs in the term for the kinetic energy in the Hamiltonian - for molecules with one and two CH_3-tops are compared, as they are determined from Raman, infra-red and microwave spectroscopy.

1.1 Introduction

In 1923 A. Smekal suggested that energy might be interchanged between radiation and matter during the scattering of light [2]. The atom or molecule would change from state l to state m, and the frequency of the quantum, ν_0, would increase or decrease by ν_{lm}, so as to conserve energy;

$$E_l + h\nu_0 = E_m + h(\nu_0 - \nu_{lm}) \tag{1.1}$$

In 1928 the Indian scientist C.V. Raman measured, together with K.S. Krishnan, scattered radiation of this type in liquid carbon tetrachloride using a mercury arc as excitation source [3]. The displaced radiation had not been observed previously because it is very weak, and the probability of scattering without change of wavelength is much higher (Rayleigh scattering)

From 1928 until the second world war, most of the rotational and vibrational spectra were obtained using Raman methods. With the development of infrared and microwave instrumentation in the fifties, interest in Raman techniques declined. It was the invention of the visible laser in the early 1960s that made physicists rediscover the Raman effect. In the late 1960s non-linear optical phenomena, i.e. hyper Rayleigh and Raman scattering and coherent anti-Stokes Raman scattering (CARS), were reported [4] and gave new impulses.

Due to improvements in lasers and detectors, new developments took place including Raman microscopy, the discovery of surface enhanced Raman spectroscopy and the use of time-resolved Raman spectroscopy. Sensitive OMAs and CCD-cameras allow the observation of Raman spectra in a short acquisition time. High power pulsed lasers made it possible to develop CARS into a powerful tool to study e.g. combustion processes [5]. Stimulated Raman gain and loss spectroscopy enabled a resolution of the order of 0.001 cm^{-1} to be achieved in the spectra of low pressure gases [6]. Lasers with pico- and femto-second pulses allows the study of very fast chemical reactions. Fourier transform Raman spectroscopy in the near infrared makes rapid progress and should permit to overcome the limitations imposed by sample fluorescence, if visible light is used.

CARS has become an important non-intrusive tool to study combustion processes [7], electric discharges, free jet expansions, photofragmentation events [8] and the chemical analysis of biological samples [9]. In [10] the advantages and disadvantages of CARS over other optical methods as a non-intrusive diagnostics tool are summarized. One of the main disadvantages is the presence of a non-resonant background (due to χ_{nr}) of diluent gases, which may swamp the Raman resonant part of the species of interest; this limits the sensitivity of CARS ($10^2 - 10^4$ ppm for most cases of interest; sensitivity can be increased by a factor 30 using polarisation CARS [7]). The main advantage is that the signal is emitted in a well-collimated beam, which makes a high signal collection efficiency possible. Also discrimination against fluorescence becomes much easier.

However, spontaneous Raman spectroscopy (SRS) is, due to its rather inexpensive experimental equipment and easy data acquisition, still one of the most favourable forms of Raman spectroscopy. In addition, the sample concentration can be calibrated in a straightforward manner. The experimental complexity of non-linear Raman spectroscopy compared to SRS justifies the thought that one should always first think of using SRS, and after that (maybe) a non-linear Raman technique.

1.2 Experimental set-up

The experimental results presented in this thesis are obtained with a spontaneous Raman setup. As an excitation source is used an Spectra Physics Ar-ion laser (model 2030-15S) with an ouput power of about 7 Watt on the 488 nm laserline. From this laser the output coupler is removed and replaced by two curved mirrors (see fig. 1). The focal distance of

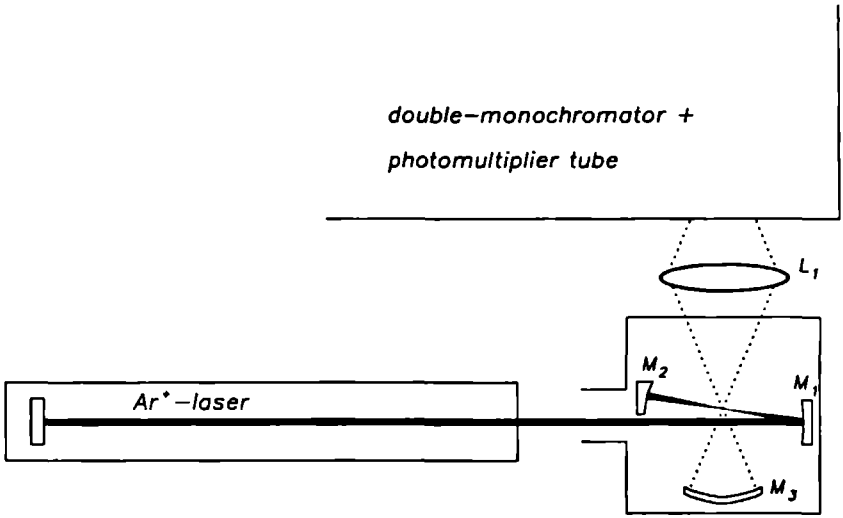

Figure 1: The experimental setup

the folding mirror (M_1) equals the radius of curvature of the mirror M_2 (50 mm). The focus produced inside the cavity has a waist, $2\omega_0$, of 50 μm if the mirrors are properly adjusted. Both mirrors are placed inside the sample cell and are adjustable from outside. In this way a factor 80 is gained in power, as compared to extracavity measurements. Since in the Raman proces the signal is linearly proportional to the power, the same factor is gained in the measured intensity of the Raman spectra. The light which leaks through the folding

mirror is measured with a photodiode. The signal from the photodiode is fed back to the power supply, which controls the current of the laser discharge. In this way the laser power is kept constant during the measurements.

The light, scattered from the molecules in the focus, is collected under 90° by a lens L_1 (f = 80 mm, D = 40 mm) and imaged on the entrance slit of a Jobin-Yvon double monochromator (model Ramanor HG-2S) which has an f/8 aperture and a dispersion of 2.5 Å/mm. Each stage consists of a concave holographically ruled grating (2000 groves/mm, $110 \times 110\,mm^2$) and two horizontally placed slits. The slits are adjustable in height ($10 - 2000\,\mu m$) and have a width of 20 mm. The entrance slit of the first and the exit slit of the second monochromator determine mainly the resolution of the instrument. The other two slits are important if one wants to suppress Rayleigh scattering; i.e. if one has to measure small Raman shifts ($< 200\,cm^{-1}$).

During the experiments, discussed in chapter two and three, a high pressure sample cell was used, which could stand pressures up to 30 bar. The working pressure was 3 bar and 0.6 bar for propane and dimethylamine, respectively, although for both gases the vapor pressures at room temperature are much higher. However, due to the formation of small droplets at higher pressure, light scattering caused severe fluctuation of the laser power.

A new cell was constructed which made it possible to perform measurements in a jet. Some preliminary jet measurements are performed and presented in [11]. In chapter 4 and 5, the jet is only used to renew the contents of the cell and not to expand the molecules. The pressure inside the cell is kept constant by pumping and flowing the gas at the same rate. Due to this flow no droplets are formed in the laser focus. The stability of the laser is very sensitive to convections; therefore, the flow has to be adjusted with care.

At the side of the laser, the cell is closed with a window under brewster-angle. The reflection from this window is focussed on the fiber. This reflection possesses the well-known Ar^+ spectrum [12], as it is emitted from the discharge in the laser tube. The exit of the fiber can be positioned on the other side of the focus, as seen from the imaging lens L_1 (in stead of mirror M_3, which increases the collection efficiency by almost a factor of 2). The 'fiber-transmitted' plasma light is sent directly into the monochromator serving for frequency calibration of the Raman spectrum. In this way also weak plasma lines become observable; one does not have to rely on the Rayleigh scattering of strong plasma lines, which are not always present in the frequency range under investigation.

The frequency selected light is measured with a photomultiplier tube at the exit of the second monochromator. The propane spectra are obtained with an EMI 9862B/350; the other spectra shown in this thesis are measured with a RCA C31034-02. In order to have a low dark pulse summation (< 10 counts/s at a current amplification of 10^6), both PMTs are operated at a temperature of about $-25°$ C. The signals from the PMT are 35 times amplified and then selected by a pulse height analyzer (ORTEC Brookdeal 5C14). The pulses are counted with a photon counting system (ORTEC Brookdeal 5C1) and handled

by an Apple II^e computer This computer also controls the scanning of the gratings

1.3 Recording devices

1.3.1 Single-channel photoelectric recording

As mentioned in section 1 2, almost all the spectra shown in this thesis are recorded with a photomultiplier tube With these tubes single photon counting becomes possible Inherent to this way of measuring is the scanning of the gratings during the recording of the spectra The scanning of the gratings puts a lower limit to the time needed to record a spectrum In order to record 100 cm^{-1} in steps of 0 2 cm ^{1} one needs at least 3 minutes and 40 seconds

Sometimes one has to make a second scan to calibrate the frequency scale, e g if it is hard to distinguish 'fiber-transmitted' plasma lines from scattered Raman signal or if the Raman spectrum of the gas is to weak to be recorded together with the Ar^+ spectrum (see section 1 2) Due to hysteresis of the scanning mechanism, it is almost impossible to put the monochromator back to the same starting position, the error in the frequency increases

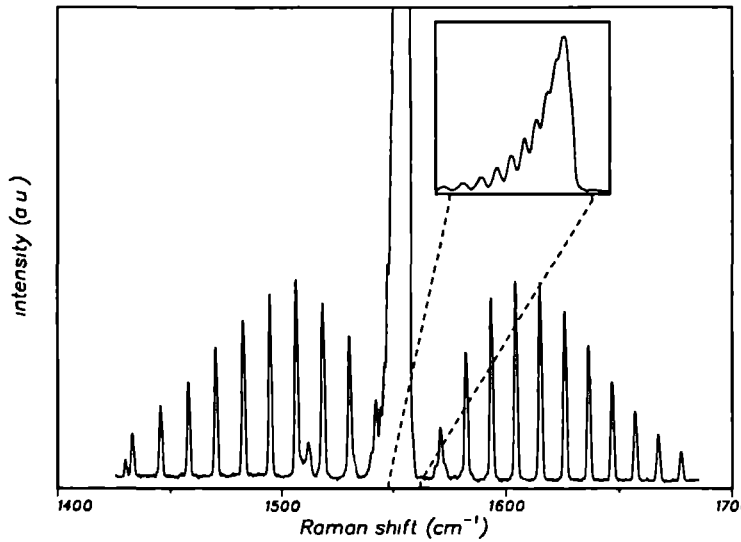

Figure 2 Part of the Raman spectrum of oxygen in air The insert shows a second measurement of the Q-branch at higher resolution (see also 1 3 1)

In figure 2 part of the Raman spectrum of air is shown The spectrum is measured with

the 514 nm laser line and 70 μm slit width; the FWHM achieved in this way is 1.0 cm^{-1}. The spectrum shows the O-, Q- and S-branch of the fundamental vibration of O_2. The Q-branch of the isotope $^{16}O^{18}O$ is clearly visible at about 1513 cm^{-1}. The insert shows part of the Q-branch of O_2 measured with the 488 nm laser line and 40 μm slit width (FWHM 0.6 cm^{-1}). It took about 1.5 hours to record the spectrum.

1.3.2 Multi-channel photoelectric recording

In the early days of Raman spectroscopy the spectra were recorded with a photographic plate. The advantage of this methode is that one can record the spectrum without moving the gratings; the frequency calibration becomes more accurate [13]. However, due to low sensitivity of the photographic plate one needs very long exposure times (15 hours is not extraordinary). The advantage of the photographic plate in recording the spectrum without scanning and the high sensitivity of the photomultiplier tube are combined in a CCD-camera. Some preliminary measurements are performed with two kinds of cameras.

The first type of camera has an image intensifier in front of a CCD-chip. The image intensifier consists of a photocathode in front of a micro channel plate (MCP). Behind the MCP is a phosphor screen, which is coupled to the CCD-chip with fiber optics (to match the size of the photocathode with the smaller CCD-chip). The chip is divided into 300×400 squares. The position on the chip determines the frequency (x-axis) and the position in space from where the light is scattered (y-axis). This camera is bought to work in a pulsed LIF set-up where flames are investigated and thus not optimized to work in a continuous Raman set-up. For example, the CCD-chip can accumulate signals only for 20 ms. The information on the chip is then read out and stored on hard-disk or video tape (about 25 pictures are stored per second). This means that for most of the Raman spectra several pictures have to be added up "softwarematically" in order to achieve a reasonable signal to noise ratio.

The size of the photocathode (ϕ 18 mm) together with the dispersion of the monochromator (2.5 Å/mm) determine the frequency range that can be detected without scanning the grating; 200 cm^{-1} can be detected in a single image of the CCD-chip. In figure 3 the fundamental vibration of hydrogen is shown, measured with this CCD-camera. During the measurement of the H_2 Raman spectrum, only the first part of the double monochromator is used. The camera is placed at the position of the exit slit of the first monochromator. The slit width was 100 μm and the pressure of the gas was 600 Torr. After 20 ms (single image) the ro-vibrational transitions, $v = 1 \leftarrow v = 0$, $\Delta J = 0$, up to $J = 3$ are clearly observed (see fig. 3). If 25 images are added up (1 second measuring time), also the transition $J' = 4 \leftarrow J'' = 4$ becomes observable.

The dynamical range of a CCD-chip is an important property; it determines the difference in strength between two signals which can just be separated. If one wants to measure

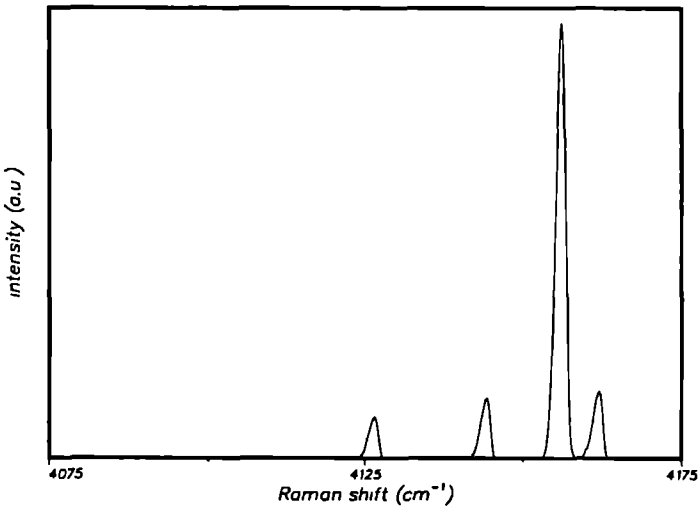

Figure 3: Raman spectrum of hydrogen measured with a CCD-camera

weak signals on a very strong flank, e.g. torsional transitions on the flank of a fundamental vibration (see chapter 2) or transitions with low Raman shifts (i.e. close to the Rayleigh line), one needs a CCD-chip with a high dynamical range ($\approx 10^5$). Signals with a difference in intensity of about $10^4 - 10^5$ are measured in the set-up described in section 1.2. The first camera had a dynamical range of 256 (8 bits), a second type of camera had a dynamical range of more than 10^5 (18 bits).

The second camera was especially designed to measure extremely low light levels. This camera consists only of a CCD-chip in a vacuum chamber, fiber-optically linked to a so-called OMA-card, which is placed inside a personal computer. The advantage over the first camera is that the light can be integrated over longer exposure times on the CCD-chip. The size of the chip is $9.7 \times 9.7\ \mathrm{mm}^2$, so only $100\ \mathrm{cm}^{-1}$ can be detected in a single image. However, 512 spectra can be added up in 5 ms., which makes it possible to detect the H_2 Raman spectrum, $v = 1 \leftarrow v = 0$, $\Delta J = 0$, up to $J = 6$ after 30 seconds of integration time.

With this camera the torsional Raman spectrum of propane was measured. After 2 minutes(!) integrating on the chip, the spectrum shown in figure 4 was measured. Compared to the spectrum shown in figure 3a in chapter 2, the same features are visible. The big difference is the time required to measure the spectrum; 2 minutes vs 8 hours. Even more time is gained if one has to measure gases for which it takes hours before the intracavity

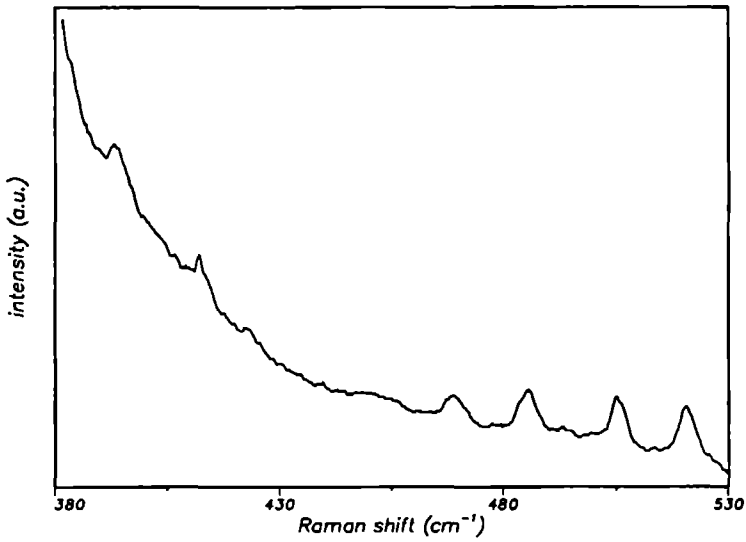

Figure 4: Torsional Raman spectrum of propane measured with a CCD-camera

laser becomes stable in power (e.g. dimethylamine). If one uses a camera the laser has to stay stable for only a few minutes, which is the case after typically 30 minutes. The part of the Raman spectrum where the $\Delta N = 4$ torsional transitions of propane were measured, was investigated as well. Here, it was necessary to add up 5 spectra each of 2 minutes integration time. It became clear that with 25 spectra added up, all the features would appear, as in figure 3b in chapter 2.

1.4 Internal motion

One distinguishes several kinds of internal motion; e.g. ring puckering, inversion motion and internal rotation. In this thesis we will mainly deal with the latter one, except in chapter 6 where the inversion motion of ammonia is discussed. One of the reasons to study internal motions is to gain insight in the origin of barriers, and to provide information to test methodes describing coupling of and rearrangements between different modes (see chapter 2). The information might as well shed some light upon the problem of structural preference.

There are two main experimental methodes to study internal motions: microwave spec-

troscopy and Raman overtone spectroscopy. In a microwave experiment overall rotational transitions are measured with high resolution and accuracy. From the effect of the internal motion on the rotational spectrum -each rotational transition will exhibit a fine structure caused by the interaction of the internal and overall rotation- one evaluates the height of the potential barrier hindering internal rotation. Raman overtone spectra possess transitions between different torsional levels, where one of the levels can be above the torsional barrier. In table 1 some torsional data on molecules with one and two methyl-like rotors, determined from MW- and IR/RAMAN-spectra, are collected. For systems where Raman and MW-data are available, rather big discrepancies can be found. In the case of propane, a recent microwave investigation [17] revealed a 20 % lower barrier parameter as determined from our Raman measurements (see chapter 2). This enormous discrepancy is clearly not caused by bad measurements or erroneous analysis of data. The source of the discrepancy might be that the analysis of microwave data for other than the most simple systems is highly complicated. Inclusion of rotor-rotor terms in the hamiltonian would make the calculation rather untractable. Consequently, microwave data are usually analyzed with truncated effective hamiltonians [18, 19]. Another problem in microwave spectroscopy might be that most of the data are on transitions in the torsional groundstate or sometimes the first excited state. These transitions can be described with a few effective parameters like the barrier height, V_3, and the reduced rotational constant, F, for the internal top. Inclusion of more parameters only demonstrates the strong correlation between them (for those low lying states) without yielding new insight [20]. In the case of Raman spectroscopy only few transitions are measured (due to the weakness of the effect) with a resolution $> 10^4$ times worse than in a MW-experiment. However, one measures transitions between torsional states (mainly $\Delta N = 2$, but also $\Delta N = 1$ and $\Delta N = 4$), where one of the levels may be above the barrier. For these levels the tunneling splitting becomes so big that even with our much worse resolution it is measurable. This splitting, which is very sensitive to the height of the barrier, makes an accurate determination of the barrier height possible.

Table 1: Comparison of torsional barrier heights determined from MW-data and IR/Raman-data (values in cm ^{1})

'ONE-CH_3-TOP' MOLECULES			'TWO-CH_3-TOP' MOLECULES		
$(CH_3)CH_3$ ethane 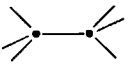			$(CH_3)CH_2(CH_3)$ propane 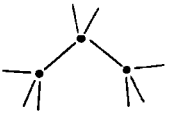		
$V_3 = 1009$	Raman[14]		$V_3 = 1353$	Raman[16]	F = 5.72
$V_3 = 1012.0$	IR[15]		$V_3 = 1108$	MW[17]	F = 6.13
$(CD_3)CD_3$ ethane-d_6					
$V_3 = 990$	Raman[21]	F = 1.3416			
$V_3 = 989$	IR[22]	F = 1.3416			
$(CH_3)NH_2$ methylamine 			$(CH_3)NH(CH_3)$ dimethylamine 		
$V_3 = 684.71$	MW[23]	F = 7.1	$V_3 = 1350$	Raman[24]	F = 6.7
$(CH_3)HC=O$ acetaldehyde 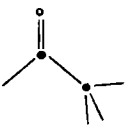			$(CH_3)_2C=O$ acetone 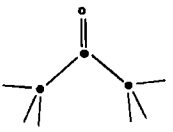		
$V_3 = 406$	MW[25]	F = 7.5	$V_3 = 279.4$	IR[26]	F = 5.73
			$V_3 = 266.3$	MW[27]	F = 5.59

Table 1 continued

'ONE-CH_3-TOP' MOLECULES			'TWO-CH_3-TOP' MOLECULES		
$(CH_3)CH=CH_2$ propene	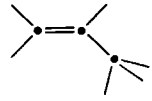		$(CH_3)HC=CH(CH_3)$ butene	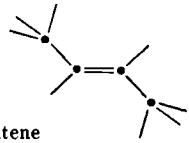	
			trans-2-butene		
$V_3 = 721.3$	Raman[28]	$F = 7.1$	$V_3 = 712.7$	IR&Raman[30]	$F = 7.05$
$V_3 = 698.4$	MW[29]	$F = 7.100$	$V_3 = 861.1$	Raman[28]	$F = 4.94$
			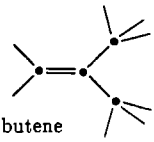		
			iso-butene		
$(CH_2)C(CH_3)(CF_3)$ 2-trifluoro- methyl- propene			$V_3 = 893.7$	IR&Raman[31]	$F = 5.77$
			$V_3 = 957.6$	Raman[28]	$F = 5.06$
			$V_3 = 759.5$	MW[32]	
			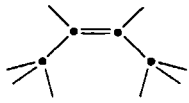		
			cis-2-butene		
$V_3 = 355$	CH_3		$V_3 = 274.6$	IR[30]	$F = 5.63$
$V_3 = 694$	CF_3	Raman[33]	$V_3 = 261$	MW[34,35]	$F = 5.69$
CH_3OH methanol	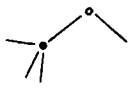		$(CH_3)O(CH_3)$ dimethylether	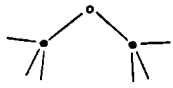	
			$V_3 = 1215$	Raman[37]	$F = 6.78$
$V_3 = 372.3$[36]			$V_3 = 916.3$	MW[38]	
CH_3SH methylmercaptan			$(CH_3)S(CH_3)$ dimethylsulfid		
$V_3 = 490$	Therm[40]		$V_3 = 804.3$	Raman[37]	$F = 5.961$
$V_3 = 400$	MW[41]		$V_3 = 747.6$	MW[39]	

1.4.1 short description of internal motion

If a molecule possesses a methyl-group connected with a single bond to the frame of the molecule, the methyl-group can "rotate", with respect to the frame, around this single bond. This motion, described by the torsional angle ϕ, is hindered, due to the interaction of the methyl-group with the frame. During the rotation of the methyl-group the potential energy varies with ϕ. The symmetry of the potential energy function is determined by the symmetry of the molecule. If during a complete revolution the molecule possesses M equivalent configurations, the potential energy function is said to have M-fold symmetry. A periodic function with period $2\pi/\mathrm{M}$, may be represented by a Fourier series expansion [20]. If one assumes minimal potential energy at $\phi = 0$, the potential function may be written as

$$V(\phi) = \tfrac{1}{2}\mathrm{V_M}(1 - \cos \mathrm{M}\phi) + \tfrac{1}{2}\mathrm{V_{2M}}(1 - \cos 2\mathrm{M}\phi) + ... \qquad (1.2)$$

1.4.2 'one-top' molecule

In the case of propene (see chapter 4) the torsional potential function has a three-fold symmetry (M = 3). In eq. 1.2, V_3 then determines the height of the barrier and V_6 alters the width. More precisely, a positive V_6-value results in a narrower potential well and a broader maximum; a negative V_6 has just the opposite effect. If the potential barrier would be infinitely high, every torsional level N (see fig. 5, N defines the number of torsional quanta in the top) is three-fold degenerate since no transmission is possible between any of the three potential wells. Due to the finiteness of the barrier, the molecule can tunnel from one well to another. This tunneling (purely a quantum-mechanical effect) through the potential barrier leads to a splitting of every torsional level N into a non-degenerate A-level and a two-fold degenerate E-level (see fig. 5). For higher excited levels the motion becomes classically allowed.

1.4.3 'two-top' molecule

For molecules which possess two methyl rotors, the energy level schema becomes somewhat more complicated (see fig. 5). Each methyl rotor experiences a three-fold hindering potential. If the height of the potential barrier would be infinite, every torsional level would be nine-fold degenerate. However, as explained above, due to the finiteness of the barrier, every level is split, in this case into one non-degenerate A-level, two two-fold degenerate E-levels and one four-fold degenerate G-level (see chapter 2). The number of torsional quanta N can be shared between the two tops. In this way torsional polyads with a fixed number of torsional quanta N can be distinguished (see fig. 5). Mutual interactions between the two methyl-tops produce extra splittings within a polyad For polyads close to and above the barrier state-mixing occurs, which renders N less meaningful.

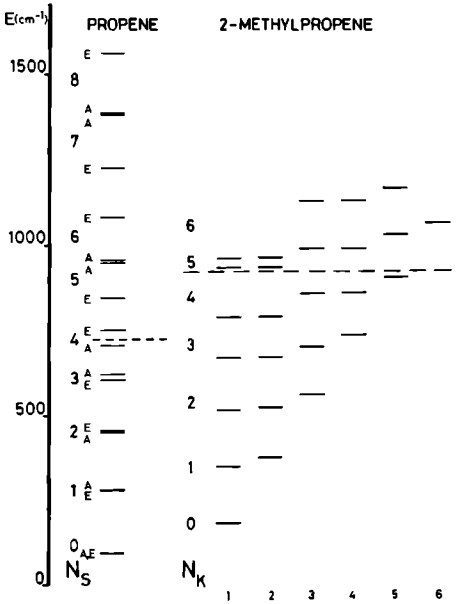

Figure 5: Energy level schema

For low lying torsional levels the splitting, due to tunnelling, can not be observed in the Raman spectra, shown in chapter 2, 3 and 4, due to the limited resolution. However, in these spectra not only transitions with $\Delta N = 2$ are observed, but sometimes also transitions with $\Delta N = 4$. The final levels are then close to or sometimes even above the barrier. For these levels the tunnelling-splitting becomes observable, even with a 2.0 cm^{-1} instrumental resolution (see chapter 2 and 3).

1.4.4 'three-top' molecule

If in ammonia one hydrogen atom is replaced by a methyl-group, mono-methylamine is formed. To form di-methylamine and tri-methylamine one has to replace two, respectively three hydrogen atoms by a methyl-group. We did not succeed in measuring the torsional Raman spectrum of mono-methylamine, because with this gas in the cell it was not possible to get the laser stable for a long time. The formation of droplets (even at low pressures < 300 Torr) caused severe fluctuation of the laser power after a few minutes already. However, the torsional spectra of di-methylamine and tri-methylamine were recorded. The analysis

of the torsional spectrum of di-methylamine is given in chapter 3. The torsional Raman spectrum of tri-methylamine is just shown here (see fig. 6), without effort to crack it. It is easy to see that the problem becomes much more complicated than in the case of two methyl rotors. To start with, every level is split into 27 sublevels, due to tunneling. Comparable to the previous two cases, they group together in one non-degenerate level, three two-fold and three four-fold degenerate levels and one eight-fold degenerate level. However, if one treats the CH_3 – groups as separate rotors ($V_3 = 3000\,cm^{-1}$, $V_6 = 250\,cm^{-1}$ and $F = 6.69\,cm^{-1}$) without any interaction, it can be demonstrated that the features in the spectra, shown in figure 6a and 6b, are torsional transitions, with $\Delta N = 1$ and $\Delta N = 2$, respectively. Here, N denotes the total number of torsional quanta chared between the three tops.

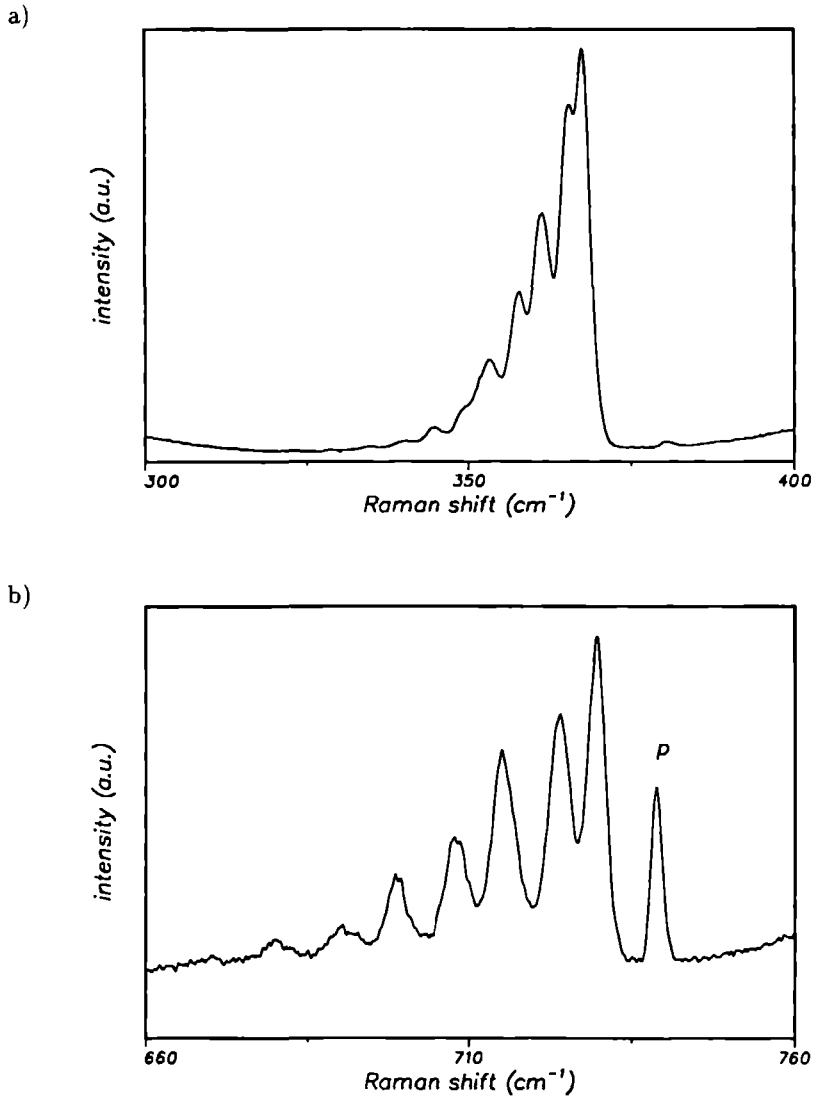

Figure 6: a) $\Delta N = 1$ and b) $\Delta N = 2$ torsional Raman spectrum of trimethylamine. P indicates a plasma line.

References

[1] D.A. Long, *Raman Spectroscopy*, McGraw-Hill, London (1977)

[2] A. Smekal, Naturwiss **11** (1923) 873

[3] C.V. Raman and K.S. Krishnan, Nature **121** (1928) 501

[4] R.W. Therhune, P.D. Maker and C.M. Savage, Phys. Rev. Letters **14** (1965) 681

[5] P.R. Regnier and J-P. Taran, Appl. Phys. Letters **23** (1973) 240

[6] A. Owyoung, R.S. McDowell and C.W. Patterson, Chem. Phys. Letters **59** (1978) 156

[7] J-P. Taran, in *Applied Laser Spectroscopy*, eds. W. Demtröder and M. Inguscio, Plenum Press, New York (1990)

[8] J.W. Nibler, in *Applied Laser Spectroscopy*, eds. W. Demtröder and M. Inguscio, Plenum Press, New York (1990)

[9] T.A.H.M. Scholten, Ph.D. thesis, University Twente (1989)

[10] J.W. Nibler and G.V. Knighten, in *Raman Spectroscopy of Gases and Liquids*, ed. A. Weber, Springer-Verlag (1979)

[11] H. Hooymayers, Internal Report, University of Nijmegen (1990), not published

[12] L. Minnhagen, Arkiv för Fysik **25** (1963) 203

[13] S. Brodersen, F. Rasmussen and J. Bendtsen, J. Raman Spectrosc. **6** (1977) 67

[14] R. Fantoni, K. van Helvoort, W. Knippers and J. Reuss, Chem. Phys. **110** (1986) 1

[15] N. Moazzen-Ahmadi, H.P. Gush, M. Halpern, H. Jagannath, A. Leung and I. Ozier, J. Chem. Phys. **88** (1988) 563

[16] R. Engeln, J. Reuss, D. Consalvo, J. van Bladel, A. van der Avoird and V. Pavlov-Verevkin, Chem. Phys. **144** (1990) 81

[17] G. Bestmann, W. Lalowski and H. Dreizler, Z. Naturforsch. **40a** (1985) 271

[18] D.R. Herschbach, J. Chem. Phys. **31** (1959) 84

[19] H. Dreizler, *Molecular Spectroscopy Modern Research*, eds. K.N. Rao and C.W. Mathews, Academic Press (1971)

[20] W. Gordy and R.L. Cooke, *Microwave Molecular Spectra*, Wiley-Interscience, New York (1970)

[21] J.M. Fernandez-Sanchez, A.G. Valdenebro and S. Montero, J. Chem. Phys. **91** (1989) 3327

[22] N. Moazzen-Ahmadi, A.R.W. McKellar, J.W.C. Johns and I. Ozier, to be published

[23] N. Ohashi, S. Tsunek. K. Takagi and J.T. Hougen, J. Mol. Spectr. **137** (1989) 33

[24] R. Engeln, J. Reuss, D. Consalvo, J. van Bladel and A. van der Avoird, Chem. Phys. Lett. **170** (1990) 206

[25] W. Liang, J.G. Baker, E. Herbst, R.A. Booker and F.C. De Lucia, J. Mol. Spectr. **120** (1986) 298

[26] P. Groner, G.A. Guirgis and J.R. Durig, J. Chem. Phys. **86** (1987) 565

[27] J.M. Vacherand, B.P. van Eijck, J. Burie and J. Demaison, J. Mol. Spectr. **118** (1986) 355

[28] R. Engeln and J. Reuss, Chem. Phys., accepted

[29] Eizo Hirota, J. Chem. Phys. **45** (1966) 1984

[30] J.R. Durig, S.D. Hudson and W.J. Natter, J. Chem. Phys. **70** (1979) 5747

[31] J.R. Durig, W.J. Natter and P. Groner, J. Chem. Phys. **67** (1977) 4948

[32] J. Demaison and H.D. Rudolph, J. Mol. Struct. **24** (1970) 231

[33] G.A. Guirgis, Y.S. Li and J.R. Durig, *Raman Spectroscopy*, eds. Lascombe and Huong, John Wiley & Sons (1982)

[34] S. Kondo, Y. Sakurai, E. Hirota and Y. Morino, J. Mol. Spectr. **34** (1970) 231

[35] confirmed by the group of Prof. Dreizler, private communications

[36] R.M. Lees, J. Chem. Phys. **59** (1973) 2690

[37] P. Groner, J.F. Sullivan and J.R. Durig, *Vibrational Spectra and Structure*, vol. 9, ed. J.R. Durig, Elsevier, Amsterdam (1981)

[38] H. Lutz and H. Dreizler, Z. Naturforsch. **33a** (1978) 1498

[39] J. Demaison, B.T. Tan, V. Typke and H.D. Rudolph, J. Mol. Spectr. **86** (1981) 406

[40] G. Herzberg, *Molecular Spectra and Molecular Structure*, vol. 2, Van Nostrand, New York (1945)

[41] C.H. Townes and A.L. Schawlow, *Microwave Spectroscopy*, McGraw-Hill, New York (1975)

Chapter 2

Torsional motion of the CH_3 groups of propane studied by Raman overtone spectroscopy

R. Engeln, J. Reuss
Department of Molecular and Laser Physics, University of Nijmegen
Toernooiveld, 6525 ED Nijmegen, The Netherlands

D. Consalvo
Dipartimento di Chimica, Universitá "La Sapienza"
P.le A. Moro 5, 00185 Roma, Italy

J.W.I. van Bladel, A. van der Avoird
Department of Theoretical Chemistry, University of Nijmegen
Toernooiveld, 6525 ED Nijmegen, The Netherlands

V. Pavlov-Verevkin
Department of Physical Chemistry, Moscow State University
119899 Moscow, USSR

Abstract

The Raman spectrum of propane is recorded between 300 and 900 cm^{-1}; first and third overtones are observed with an Ar^+ laser intracavity set-up. This spectrum is analyzed by means of a model with two hindered and coupled methyl rotors. Since the levels probed extend to the region above the torsional barrier ($V_3 = 1353\,cm^{-1}$), all the relevant molecular parameters, in particular the coupling between the methyl rotors, could be accurately determined. By means of a classical approach we have obtained further insight in the qualitative structure of the torsional spectrum.

2.1 Introduction

For a molecule like $H_3C\text{-}X\text{-}CH_3$, the interaction between the two methyl tops seems to be an elusive property. Both tops are equivalent and hindered in their rotation by a three-fold potential barrier. In 1981 Durig has discussed a number of two-top molecules [1]. Whereas the barrier height seemed to be well determined at that time, fine details could not be extracted due to the fact that *a*) most spectra were obtained for transitions between relatively low lying states (with respect to the barrier) and *b*) strong correlations between certain potential parameters were observed for these low lying states. One of the molecules treated by Durig is propane [2], for which the barrier height is about 1300 cm^{-1}. The mainly used experimental technique was overtone-Raman-spectroscopy, supplemented by some low resolution IR-absorption measurements. Both methods produce results without rotational structure.

For our purposes, i.e. to determine the torsional part of the potential, these coarse techniques are quite useful. Our new asset consists of a significantly increased sensitivity. For low lying states the torsional motion resembles a vibration around the position of one of the 3x3 potential minima. For highly excited states, i.e. above the potential barrier, the character changes to that of hindered rotations.

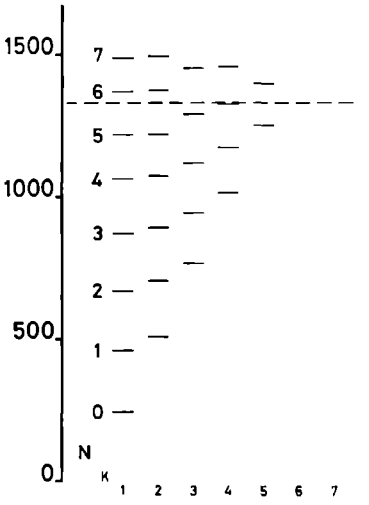

Figure 1: Energy level scheme, for levels with A-symmetry, neglecting tunneling splitting. The dashed line indicates the height of the torsional potential barrier for one top.

In fig. 1 an energy level scheme is shown, based upon our experimentally determined parameters, which will be discussed below. This scheme can serve for an introductory discussion as well. First, we define as a torsional polyad (TP) all levels with the same number of torsional quanta N, distributed as they might be over the two torsional degrees of freedom, $N = v_1 + v_2$. Polyad N consists of $N + 1$ levels. For the highest levels shown these polyads start to mix. For our purposes, however, it turns out to be a very practical classification scheme.

Except for trivial anharmonicity effects, the splittings shown in fig. 1 are mainly due to the interaction between the two tops. We shall call this splitting interaction splitting to distinguish it from tunneling splitting, which cannot be deduced from fig. 1. In view of our limited spectral resolution with a FWHM of about 0.7 cm ^{1}, the latter becomes measurable only for the higher levels.

Our experimental method consists of a refinement of Durig's measurements; to this end the gas sample is put at the position of a sharp intracavity focus of an Ar^{+}-laser. Moreover, the sample cell is constructed so that one can work at elevated pressures to gain Raman signal. In addition to eight $\Delta N = 2$ Raman transitions, we found with these improvements six $\Delta N = 4$ Raman transitions, with most of the final levels above the energy barrier, as indicated in fig. 1. Note that the $\Delta N = 4$ transitions are about 50 times weaker than strong $\Delta N = 2$ transitions. The work forms a continuation of measurements on C_2H_6 and H_3CCD_3 published previously [3,4,5].

2.2 Experimental set-up

The experimental set-up has already been described before [6,7]. It consists of an Ar^{+}-laser (Spectra Physics, model 2030-15S) from which the output mirror is removed and replaced by two highly reflecting curved mirrors (R = 50 mm, R = 100 mm), placed adjustably inside the high pressure sample cell. By changing from an extracavity to an intracavity set-up we gained a factor of 80 in Raman intensity. An intracavity power of 300 Watts could be achieved for the 488 nm laser line. The laserpower is stabilized by controlling the light which leaks through the folding mirror (R = 100 mm) of the cavity. This signal is fed back to the power supply, which controls the current of the discharge.

The high pressure cell is constructed to stand pressures up to 30 bars. The scattered Raman light, produced in the laserfocus (waist of $2w_0 = 50\ \mu m$), is collected under 90° with respect to the beam propagation and laser polarization. The focus is imaged by an f/8 lens on the entrance slit of a double monochromator (Jobin Yvon Ramanor HG2S). The four slits of this monochromator are all electronically adjustable. The measurements are performed at a resolution of 0.7 cm^{-1} (e.g. 50 μm slitwidth) for the strong transitions ($\Delta N = 2$) and 2.0 cm ^{1} (e.g. 200 μm slitwidth) for the weak transitions ($\Delta N = 4$). On the opposite side of the focus there is a curved mirror, which reflects the scattered light back to the focus. In

this way we gain almost a factor of two in collection efficiency.

The light is measured with a cooled EMI 9862B/350 photomultiplier, which has a S20 spectral response. The output data of the PMT is handled, via a photon counting system (Ortec Brookdeal 5C1), by an Apple IIe computer. This computer also controls the scanning of the gratings of the double monochromator. The frequency is calibrated to several Ar^+-transitions from the discharge inside the lasertube, which are measured during the scan [8]. The accuracy achieved in this way is 0.3 cm^{-1} for the $\Delta N = 4$ transitions and 0.1 cm^{-1} for the strongest $\Delta N = 2$ transitions.

The experiments are performed in bulk at a pressure of 3 bar. For higher pressure, light scattering caused severe fluctuations of the power level of the Ar^+-laser. The propane was purchased from J.T. Baker with a 99.5% purity. The Raman spectra are recorded with a scan velocity of 40 cm^{-1}/hour for the $\Delta N = 2$ transitions and 8 cm^{-1}/hour for the $\Delta N = 4$ transitions.

2.3 Theoretical aspects

The molecular symmetry group of propane is $G_{36} \simeq (C_3 \otimes C_3) \wedge (C_2 \otimes C_s)$ [1,9,10], where $\otimes$ denotes the direct and $\wedge$ the semi-direct product of the subgroups. The character table of G_{36} is given by Bunker [9]. The Hamiltonian for the non-rotating ($J = 0$) propane molecule can be written as

$$\hat{H} = F(\hat{P}^2_{\alpha_1} + \hat{P}^2_{\alpha_2}) + F'\hat{P}_{\alpha_1}\hat{P}_{\alpha_2} + V(\alpha_1, \alpha_2) \qquad \alpha_1,\ \alpha_2 \in [-\pi,\ \pi\rangle, \tag{2.1}$$

with the following Fourier expansion, up to sixth order, for the potential

$$\begin{aligned} V(\alpha_1, \alpha_2) \;=\; & \sum_{k=1,2} \left[\tfrac{1}{2}V_3(1 - \cos 3\alpha_k) + \tfrac{1}{2}V_6(1 - \cos 6\alpha_k)\right] \\ & + \tfrac{1}{2}V_+\big(1 - \cos(3\alpha_1 + 3\alpha_2)\big) + \tfrac{1}{2}V_-\big(1 - \cos(3\alpha_1 - 3\alpha_2)\big). \end{aligned} \tag{2.2}$$

The angles α_1 and α_2 describe the torsions about the C C bonds (see fig. 2). These angles are taken to be zero if a predetermined hydrogen atom of the top lies in the C-C C plane. The momenta conjugate to the torsional angles are $\hat{P}_{\alpha_1} = -\imath\frac{\partial}{\partial\alpha_1}$ and $\hat{P}_{\alpha_2} = -\imath\frac{\partial}{\partial\alpha_2}$. The parameters V_3 and V_6 describe the top-frame interaction, whereas V_+ and V_- describe the anti-geared and geared top-top interactions. The coefficients F and F' are determined by the geometrical properties of the molecule only [11]. However, because we do not want to rely on a fixed geometry, these coefficients are taken to be parameters, which are optimized as described below, just as the potential parameters V_3, V_6, V_+ and V_-. It can be readily seen that the Hamiltonian given by eq. (2.1) is indeed invariant under all operations of G_{36}

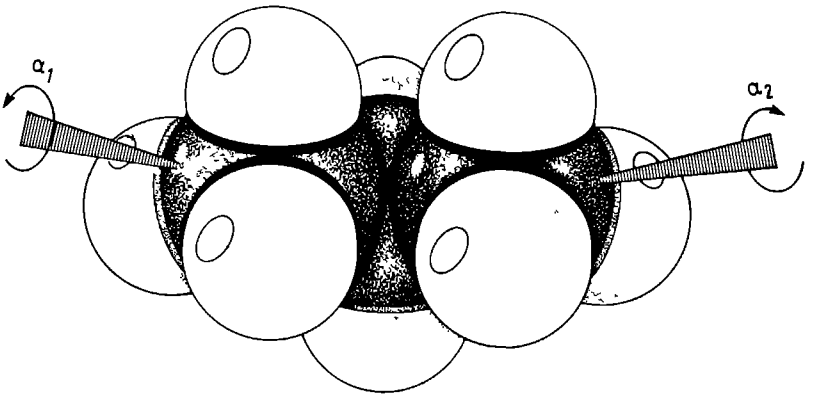

Figure 2: Equilibrium geometry and torsional angles α_1 and α_2 for propane. Note that positive α_k are defined clockwise as seen from the central C-atom.

Our notation is somewhat different from that used by Durig *et al* [2] The correspondence can be expressed by $F = \frac{1}{2}\hbar^2 g^{44} = \frac{1}{2}\hbar^2 g^{55}$, $F' = \hbar^2 g^{45}$, $V_3 = V_{30} = V_{03}$, $V_6 = V_{60} = V_{06}$, $V_+ = \frac{1}{2}(V'_{33} - V_{33})$ and $V_- = -\frac{1}{2}(V'_{33} + V_{33})$.

The Hamiltonian $\hat{H}$ can be separated into three parts:

$$\hat{H} = \hat{H}_1 + \hat{H}_2 + \hat{H}_{12}, \tag{2.3}$$

where

$$\hat{H}_k = F\hat{P}^2_{\alpha_k} + \tfrac{1}{2}V_3(1 - \cos 3\alpha_k) + \tfrac{1}{2}V_6(1 - \cos 6\alpha_k) \quad (k = 1, 2), \tag{2.4}$$

and

$$\hat{H}_{12} = F'\hat{P}_{\alpha_1}\hat{P}_{\alpha_2} + \tfrac{1}{2}V_+\big(1 - \cos(3\alpha_1 + 3\alpha_2)\big) + \tfrac{1}{2}V_-\big(1 - \cos(3\alpha_1 - 3\alpha_2)\big). \tag{2.5}$$

In order to diagonalize $\hat{H}$, we first diagonalize $\hat{H}_k$ (single-top problem) in the orthonormal basis

$$\psi_{3n_k+\sigma_k}(\alpha_k) = (2\pi)^{-1/2} \exp\left[i(3n_k + \sigma_k)\alpha_k\right], \tag{2.6}$$

with $\sigma_k = 0, \pm 1$ and $n_k = 0, \pm 1, \ldots, \pm n_{\max}$. The use of σ_k is convenient because the basis functions for a given σ_k span the irreducible representations (irreps) Γ^1 ($\sigma_k = 0$), Γ^2 ($\sigma_k = -1$) and $\Gamma^3 = \Gamma^{2*}$ ($\sigma_k = 1$) of the subgroup C_3 of G_{36}. In this way we achieve a block factorization of the Hamiltonian matrix into three blocks. Note that the above diagonalization needs to be carried out only once, because $\hat{H}_1$ and $\hat{H}_2$ have identical forms.

Taking into account only the lowest $v_{\max}$ eigenvectors A^{v_k} of the single-top problem, which are real, we can create an orthonormal basis $\varphi^{v_1\,v_2}_{\sigma_1\,\sigma_2}$ for the total two-top Hamiltonian $\hat{H}$

$$\phi^{v_1\,v_2}_{\sigma_1\,\sigma_2}(\alpha_1,\alpha_2) = \sum_{n_1,n_2} A^{v_1}_{3n_1+\sigma_1}\, A^{v_2}_{3n_2+\sigma_2}\, \psi_{3n_1+\sigma_1}(\alpha_1)\, \psi_{3n_2+\sigma_2}(\alpha_2), \tag{2.7}$$

with $\sigma_k = 0, \pm 1$ and $v_k = 0, \ldots, v_{\max} - 1$ $(k = 1, 2)$, where v_k denotes the number of torsional quanta present in the k^{th} rotor. From these basis functions we can project bases of the irreps of G_{36} (see table 1), giving 16 blocks in the Hamiltonian matrix. Diagonalizing

Table 1: Bases of irreps of G_{36}

irrep of G_{36}	basis	
A_1	$\phi^{v_1\,v_2}_{0\,0}$	$(v_1 = v_2)$
	$\frac{1}{2}\sqrt{2}\,(\phi^{v_1\,v_2}_{0\,0} + \phi^{v_2\,v_1}_{0\,0})$	$(v_1 > v_2,\ v_1 + v_2$ even$)$
A_2	$\frac{1}{2}\sqrt{2}\,(\phi^{v_1\,v_2}_{0\,0} - \phi^{v_2\,v_1}_{0\,0})$	$(v_1 > v_2,\ v_1 + v_2$ odd$)$
A_3	$\frac{1}{2}\sqrt{2}\,(\phi^{v_1\,v_2}_{0\,0} + \phi^{v_2\,v_1}_{0\,0})$	$(v_1 > v_2,\ v_1 + v_2$ odd$)$
A_4	$\frac{1}{2}\sqrt{2}\,(\phi^{v_1\,v_2}_{0\,0} - \phi^{v_2\,v_1}_{0\,0})$	$(v_1 > v_2,\ v_1 + v_2$ even$)$
E_1	$\phi^{v_1\,v_2}_{1\,1},\ \phi^{v_2\,v_1}_{1\,1}$	$(v_1 = v_2)$
	$\frac{1}{2}\sqrt{2}\,(\phi^{v_1\,v_2}_{1\,1} + \phi^{v_2\,v_1}_{1\,1}),\ \frac{1}{2}\sqrt{2}\,(\phi^{v_1\,v_2}_{1\,1} + \phi^{v_2\,v_1}_{1\,1})$	$(v_1 > v_2)$
E_2	$\frac{1}{2}\sqrt{2}\,(\phi^{v_1\,v_2}_{1\,1} - \phi^{v_2\,v_1}_{1\,1}),\ \frac{1}{2}\sqrt{2}\,(\phi^{v_1\,v_2}_{1\,1} - \phi^{v_2\,v_1}_{1\,1})$	$(v_1 > v_2)$
E_3	$\phi^{v_1\,v_2}_{1\,1},\ \phi^{v_2\,v_1}_{1\,1}$	$(v_1 = v_2)$
	$\frac{1}{2}\sqrt{2}\,(\phi^{v_1\,v_2}_{1\,1} + \phi^{v_2\,v_1}_{1\,1}),\ \frac{1}{2}\sqrt{2}\,(\phi^{v_1\,v_2}_{1\,1} + \phi^{v_2\,v_1}_{1\,1})$	$(v_1 > v_2)$
E_4	$\frac{1}{2}\sqrt{2}\,(\phi^{v_1\,v_2}_{1\,1} - \phi^{v_2\,v_1}_{1\,1}),\ \frac{1}{2}\sqrt{2}\,(\phi^{v_1\,v_2}_{1\,1} - \phi^{v_2\,v_1}_{1\,1})$	$(v_1 > v_2)$
G	$\phi^{v_1\,v_2}_{1\,0},\ \phi^{v_2\,v_1}_{0\,1},\ \phi^{v_2\,v_1}_{0\,1},\ \phi^{v_1\,v_2}_{1\,0}$	

these blocks yields the eigenstates of the system. The eigenstates can now conveniently be labelled by $|\nu\,\Gamma\rangle$, where Γ is an irrep of G_{36} and ν a quantum number labelling the different states belonging to Γ.

In order to obtain the relative Raman intensities [12], we calculate the transition matrix elements $\langle\nu'\,\Gamma|\,\alpha\,|\nu\,\Gamma\rangle$ between the eigenstates $|\nu\,\Gamma\rangle$ obtained previously. For the isotropic polarizability α we assume the following dependence on the torsional angles (the first non-vanishing terms in the Fourier expansion)

$$\alpha \propto \cos(3\alpha_1) + \cos(3\alpha_2). \tag{2.8}$$

The results are compared directly to the measured relative intensities, thus neglecting the effect of the anisotropy in the polarizability. The eigenstates $|\nu\,\Gamma\rangle$ are occupied according

to a Boltzmann distribution at $T = 300$ K. Because the isotropic polarizability is an irreducible tensor operator of rank zero (scalar) it belongs to the irrep A_1 of G_{36}. As a consequence it can only induce Raman transitions between levels belonging to the same irrep of G_{36}. To obtain the parameters in the Hamiltonian (eq. (2.1)) from the experimental spectrum we minimized the squared difference between the calculated frequencies $\nu_i^{\rm calc}$ and the experimental frequencies $\nu_i^{\rm exp}$, where i corresponds to the transition $|\nu\,\Gamma\rangle \rightarrow |\nu'\,\Gamma\rangle$, considering the expression

$$\left[\sum_i \left((\nu_i^{\rm calc} - \nu_i^{\rm exp}) \cdot w_i\right)^2\right]^{1/2} \tag{2.9}$$

The weight factors w_i are taken to be the inverse of the experimental uncertainties.

The error in the parameters is determined in the following way. Starting from the frequencies $\nu_i^{\rm exp}$, we shift these frequencies by a random amount Δ_i within the experimental error range of that specific frequency. With the new frequencies $\nu_i^{\rm exp} + \Delta_i$ a new set of parameters has been obtained using the above mentioned minimization procedure. If this process is repeated a number of times the error in a certain parameter will equal the standard deviation of the values generated for that parameter.

If we consider propane as a nearly-rigid molecule (as in section 2.5), its molecular symmetry group would be $G_4 \simeq C_2 \otimes C_s \simeq C_{2v}$. The torsional motions become normal vibrations of type A_2 and B_1 within this group. The levels N_K (see fig. 1), given by these normal vibrations, can be labelled within the group G_4 as

$$\Gamma_{N_K} = (A_2)^{N-K+1} \otimes (B_1)^{K-1} = \begin{cases} A_1 & N \text{ even, } K \text{ odd} \\ A_2 & N \text{ odd, } K \text{ odd} \\ B_1 & N \text{ odd, } K \text{ even} \\ B_2 & N \text{ even, } K \text{ even} \end{cases} \tag{2.10}$$

The reverse correlation [9] between G_4 and G_{36} (table 2) makes it easy to indicate the correlation between the levels N_K and the eigenkets $|\nu\,\Gamma\rangle$.

Table 2: Reverse correlation between G_4 and G_{36}

G_4	G_{36}
A_1	$A_1 \oplus E_1 \oplus E_3 \oplus G$
A_2	$A_3 \oplus E_2 \oplus E_3 \oplus G$
B_1	$A_2 \oplus E_1 \oplus E_4 \oplus G$
B_2	$A_4 \oplus E_2 \oplus E_4 \oplus G$

2.4 Results and discussion

In fig 3 we show the two parts of the spectrum where the torsional transitions are measured On the left side of fig 3a the ν_9 C–C–C bending mode at 369 6 cm^{-1}, which is very intense compared to the torsional overtone transitions, causes a steep rise In the frequency range 530-675 cm^{-1} no torsional overtone transitions were observed The torsional transitions in

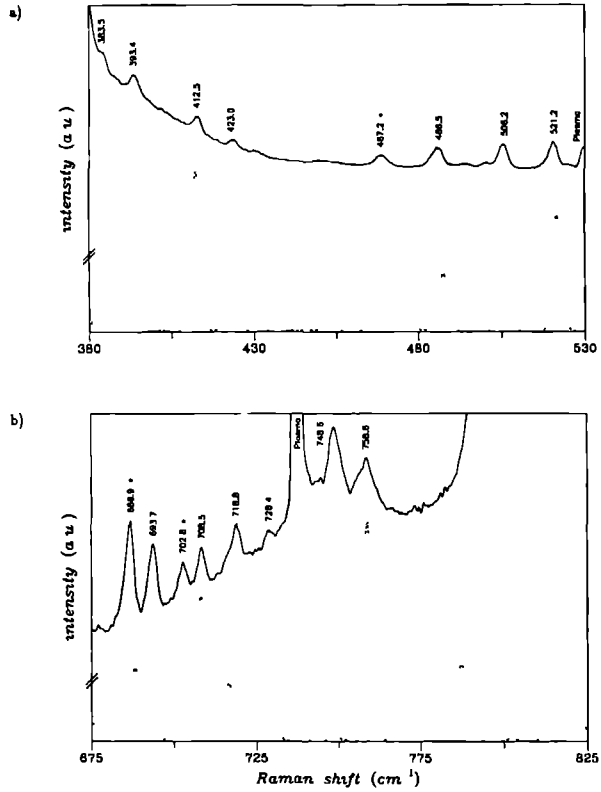

Figure 3 Raman spectra of propane for the a) $\Delta N = 2$ and b) $\Delta N = 4$ transitions The solid lines represent the experimental spectra and the dashed lines the theoretical spectra with a FWHM of 3 2 cm^{-1} In fig a the highest (lowest) experimental intensity corresponds with 12000 (400) counts In fig b the corresponding numbers are 3200 and 2300

Table 3 Observed and calculated frequencies, $n_{max} = 15$, $v_{max} = 10$, and intensities of torsional Raman overtone transitions (cm^{-1})

observed Raman shift	observed intensity[1]	assignment[2]	calculated Raman shift	calculated intensity
369 6(1)	–	ν_9^{CCC}–bend	–	–
383 5(3)	[3]	$1_2 \rightarrow 3_2$	383 23	0 46
393 4(2)	0 54	$2_1 \rightarrow 4_1$	393 58	0 95
412 5(1)	0 48	$1_1 \rightarrow 3_1$	412 39	1 38
423 0(1)	0 25	$0_1 \rightarrow 2_1$	423 05	1 43
467 2(2)*	0 65	$2_2 \rightarrow 4_4$	468 61	0 35
		$3_4 \rightarrow 5_6$		
486 5(2)	1 02	$1_1 \rightarrow 3_3$	487 56	0 57
		$2_3 \rightarrow 4_5$		
506 2(1)	0 89	$1_2 \rightarrow 3_4$	505 62	0 82
521 2(1)	1 00	$0_1 \rightarrow 2_3$	521 61	1 00
686 9(3)*	0 64 10 [1]	$2_3 \rightarrow 6_3(E_1, E_3, G)$	688 19	0 45 10^{-1}
		$3_1 \rightarrow 6_1(A_3)$		
		$3_1 \rightarrow 6_2(G)$		
693 7(3)[4]	–	–	–	–
702 8(3)*	0 15 10^{-1}	$2_1 \rightarrow 6_1(E_3)$	703 32	0 83 10^{-1}
		$2_1 \rightarrow 6_2(G)$		
708 5(3)	0 16 10^{-1}	$1_2 \rightarrow 5_2(E_1, E_4)$	708 21	0 97 10^{-1}
		$2_1 \rightarrow 6_1(E_1)$*		
718 8(3)*	0 21 10 [1]	$3_2 \rightarrow 7_4(A_2)$[5]	716 56	0 35 10^{-1}
		$3_2 \rightarrow 7_3(G)$[5]		
		$2_3 \rightarrow 7_1(E_3)$[5]		
728 4(3)	0 62 10^{-2}	$1_2 \rightarrow 5_2(A_2, G)$	728 82	0 34 10^{-1}
736 0(5)[4]	–		–	–
748 6(3)[4]	–	–	–	–
758 6(3)	0 38 10^{-1}	$1_1 \rightarrow 5_1(E_2, E_3, G)$	758 92	0 13

* not used in the fit

1 relative to the $0_1 \rightarrow 2_3$

2 the notation is explained in section 2 4 if Γ is not specified, the 4 Γ blocks lead to undistinguishable transitions

3 shoulder (see fig 3a)

4 possible ν_9 combination band (see section 2 4)

5 the 7_1 level contains a strong admixture from the 6th polyad therefore, this transition, which does not seem to be a $\Delta N = 4$ one, is allowed For the same reason, the assignment of N becomes somewhat arbitrary for the 7_3 and 7_4 levels

fig. 3b are measured on the flank of the ν_8 fundamental vibration of propane. The steep rise on the right is caused by an iso-butane impurity in the sample. The first calculations have been performed for the strongest $\Delta N = 2$ transitions. The parameters of the Hamiltonian (eq. (2.1)) thus found have been used to predict the torsional Raman spectrum. The final assignment for the measured transitions and the differences between observed and calculated frequencies are listed in table 3. For the assignment we use the notation N_K, in which N describes the polyad and K one of the $N+1$ levels in the polyad (see fig. 1 and table 5).

The transitions marked with an asterisk have not been used to fit the parameters of the torsional hamiltonian in eq. (2.1). The reason is that the observed peaks are composed of two or more transitions with different intensity; the intensities can only be estimated using eq. (2.8). In the calculated spectra of figs. 3a and 3b the corresponding peaks are the sum of the estimated intensities. All parameters found from this fit and used to calculate the torsional Raman spectrum are listed in table 4. The values for the kinetic coefficients F and F' are in reasonable agreement with the values of Durig *et al.* [2], calculated from an assumed structure. Note that our F' corresponds to $\hbar^2 g^{45}$ of [2].

Table 4: Torsional potential constants and kinetic coefficients (cm^{-1})

	value[1]	error	value[2]	error
V_3	1353	2	1323.4	9.6
V_6	18.9	0.5	-	-
V_+	-143	2	-154.3[3]	7.8
V_-	-40.4	0.8	-22.3[3]	7.8
F	5.72	0.01	6.1021[4]	-
F'	-1.58	0.02	-1.4335[4]	-

1. our result (see section 2.4)
2. Durig *et al.* [2]
3. see section 2.3
4. calculated from an assumed structure by Durig *et al.* [2]

Fig. 4 shows equipotential curves on the potential surface in α_1 and α_2. From eq. (2.2) it is clear that the potential is symmetric with respect to the reflections $\alpha_1 \rightleftharpoons \alpha_2$ and $\alpha_1 \rightleftharpoons -\alpha_2$, because the corresponding operations belong to G_{36}. From fig. 4 it seems that the potential is also symmetric with respect to the reflections $\alpha_1 \rightleftharpoons -\alpha_1$ or $\alpha_2 \rightleftharpoons -\alpha_2$. This is only approximately so, because the corresponding operations do not belong to G_{36}.

In fig. 5 four probability densities of eigenfunctions of the torsional hamiltonian (eq. (2.1)) are drawn, superimposed on the potential surface of fig. 4. The eigenfunctions belonging to the figs. 5a,b and 5c,d have energies close to and well below V_3, respectively. In figs. 5c

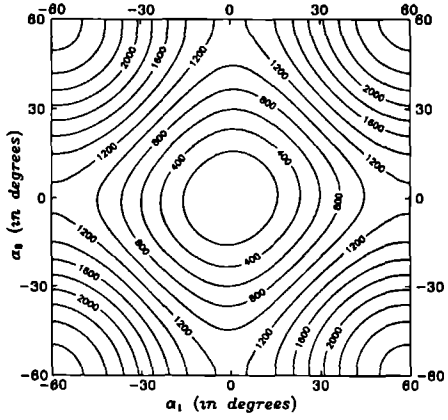

Figure 4: Torsional potential for propane. The numbers indicating the contour lines are energy values in wavenumbers.

and 5d the molecule wiggles around the potential minimum. When the energy is close to the torsional barrier, the molecule can tunnel through the barrier and move from one well to another.

The eigenfunctions are symmetric or antisymmetric with respect to exchange of excitation between rotor 1 and 2 (besides those belonging to $\Gamma = G$, see table 1). For instance, to the levels 1_1 and 1_2 of $\sigma_1 = \sigma_2 = 0$ ($\Gamma = A_3$ and A_2, resp.) belong with high accuracy the eigenfunctions $\frac{1}{2}\sqrt{2}[|1\,0\rangle \pm |0\,1\rangle]$. Here, $|v_1\,v_2\rangle = |1\,0\rangle$ indicates one torsion quantum in rotor 1 and zero in rotor 2 (see figs. 5c,d). For higher levels the situation becomes more complex, since many more states of the type $|v_1\,v_2\rangle$ contribute to the eigenfunctions. However, for increasing excitation, the lowest levels of a polyad regain part of their simplicity, due to the anharmonicity of the single rotor barrier potential. For instance, the $|5\,0\rangle$ excitation is degenerate with the $|0\,5\rangle$ excitation, but not with the $|4\,1\rangle$ or $|3\,2\rangle$ ones. This regained simplicity is shown in figs. 5a,b. The $5_1(A_3)$-level possesses an eigenfunction whose probability density shows 6 maxima along the α_1-axis; i.e. the 5 nodes of a $|5\,0\rangle$ excitation are present. Fig. 5a is symmetric with respect to exchange $\alpha_1 \rightleftharpoons \alpha_2$; therefore, the same 5 nodes are visible along the α_2-axis. The V_+- and V_--terms slightly distort the picture in the sense that both α_1 and α_2 being positive or negative corresponds to a preferred situation. Fig. 5b corresponds to the antisymmetric case. Therefore, along the diagonal $\alpha_1 = \alpha_2$ one finds a vanishing probability. Except for this main change, the figures look very similar.

From fig. 1 it can be seen that the average energies of the torsional levels of the different polyads start to come closer together as the energy of the polyads approaches the barrier

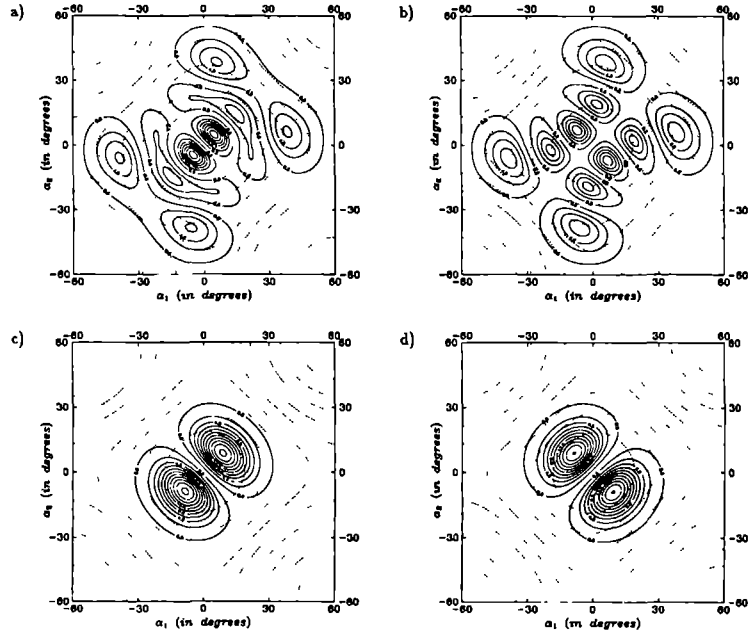

Figure 5: Probability density (multiplied by $4\pi^2$) for four wavefunctions, a) $5_1(A_3)$, b) $5_2(A_2)$, c) $1_1(A_3)$ and d) $1_2(A_2)$ (solid lines), superimposed on the potential surface (dashed lines). The solid contour lines are equidistant in the probability density and start for all figures at the same value.

top. This is in accordance with what is found for H_3CCH_3 and H_3CCD_3 [3,4]. We expect the levels far above the barrier to behave like rotational levels.

It is also evident from fig. 1 that the lowest levels of each polyad tend to group into pairs of nearly degenerate levels, for higher excitation. The remaining splitting ΔE determines the time, $\tau = \hbar/\Delta$E, a molecule needs to get the torsional excitation transferred from one end of the molecule to the other, if one starts from a situation in which one of the two rotors is excited. The higher the excitation the longer this transfer-time. For instance, τ changes from 0.1 ps for N=1 to 1 ps for N=6. This transfer rate depends on the molecule in question. For propane, the intermediate CH_2 group and the molecular dimensions determine the rate of the top-top energy transfer.

Table 5: $|\nu\ \Gamma\rangle$ representation for the torsional levels, with their calculated energies, $n_{max} = 15$, $v_{max} = 10$. The levels are ordered according to the symmetry classification of section 2.3.

N_K				
0_1	$\|0\ A_1\rangle$	$\|0\ E_1\rangle$	$\|0\ E_3\rangle$	$\|0\ G\rangle$
	246.37	246.37	246.37	246.37
1_1	$\|0\ A_3\rangle$	$\|0\ E_2\rangle$	$\|1\ E_3\rangle$	$\|1\ G\rangle$
	460.05	460.05	460.05	460.05
1_2	$\|0\ A_2\rangle$	$\|1\ E_1\rangle$	$\|0\ E_4\rangle$	$\|2\ G\rangle$
	510.94	510.94	510.94	510.94
2_1	$\|1\ A_1\rangle$	$\|2\ E_1\rangle$	$\|2\ E_3\rangle$	$\|3\ G\rangle$
	669.42	669.43	669.43	669.42
2_2	$\|0\ A_4\rangle$	$\|1\ E_2\rangle$	$\|1\ E_4\rangle$	$\|4\ G\rangle$
	705.95	705.97	705.97	705.96
2_3	$\|2\ A_1\rangle$	$\|3\ E_1\rangle$	$\|3\ E_3\rangle$	$\|5\ G\rangle$
	767 97	767.98	767.98	767.97
3_1	$\|1\ A_3\rangle$	$\|2\ E_2\rangle$	$\|4\ E_3\rangle$	$\|6\ G\rangle$
	872.53	872.38	872.38	872.46
3_2	$\|1\ A_2\rangle$	$\|4\ E_1\rangle$	$\|2\ E_4\rangle$	$\|7\ G\rangle$
	894.35	894.05	894.05	894.20
3_3	$\|2\ A_3\rangle$	$\|3\ E_2\rangle$	$\|5\ E_3\rangle$	$\|8\ G\rangle$
	946.03	945.81	945.81	945.92
3_4	$\|2\ A_2\rangle$	$\|5\ E_1\rangle$	$\|3\ E_4\rangle$	$\|9\ G\rangle$
	1016.61	1016.53	1016.53	1016.57
4_1	$\|3\ A_1\rangle$	$\|6\ E_1\rangle$	$\|6\ E_3\rangle$	$\|10\ G\rangle$
	1061.66	1063.80	1063.80	1062.53
4_2	$\|1\ A_4\rangle$	$\|4\ E_2\rangle$	$\|4\ E_4\rangle$	$\|11\ G\rangle$
	1068.92	1071.91	1071.91	1070.60
4_3	$\|4\ A_1\rangle$	$\|7\ E_1\rangle$	$\|7\ E_3\rangle$	$\|12\ G\rangle$
	1119.19	1120.77	1120.77	1119.98
4_4	$\|2\ A_4\rangle$	$\|5\ E_2\rangle$	$\|5\ E_4\rangle$	$\|13\ G\rangle$
	1175.52	1176.40	1176.40	1175.96
4_5	$\|5\ A_1\rangle$	$\|9\ E_1\rangle$	$\|9\ E_3\rangle$	$\|16\ G\rangle$
	1255.37	1255.95	1255.95	1255.66
5_1	$\|3\ A_3\rangle$	$\|6\ E_2\rangle$	$\|8\ E_3\rangle$	$\|14\ G\rangle$
	1238.58	1219.00	1218.78	1219.18

N_K				
5_2	$\|3\ A_2\rangle$	$\|8\ E_1\rangle$	$\|6\ E_4\rangle$	$\|15\ G\rangle$
	1240.20	1219.39	1219.61	1239.39
5_3	$\|4\ A_3\rangle$	$\|7\ E_2\rangle$	$\|10\ E_3\rangle$	$\|17\ G\rangle$
	1298.97	1294.63	1294.63	1296.68
5_4	$\|4\ A_2\rangle$	$\|10\ E_1\rangle$	$\|7\ E_4\rangle$	$\|19\ G\rangle$
	1333.24	1327.67	1327.67	1330.51
5_5	$\|5\ A_3\rangle$	$\|9\ E_2\rangle$	$\|12\ E_3\rangle$	$\|21\ G\rangle$
	1396.18	1399.99	1399.98	1398.24
5_6	$\|5\ A_2\rangle$	$\|13\ E_1\rangle$	$\|10\ E_4\rangle$	$\|24\ G\rangle$
	1483.87	1480.97	1483.28	1483.65
6_1	$\|6\ A_1\rangle$	$\|11\ E_1\rangle$	$\|11\ E_3\rangle$	$\|18\ G\rangle$
	1321.04	1375.57	1370 05	1320.91
6_2	$\|3\ A_4\rangle$	$\|8\ E_2\rangle$	$\|8\ E_4\rangle$	$\|20\ G\rangle$
	1320.78	1370.06	1375.58	1372.73
6_3	$\|7\ A_1\rangle$	$\|12\ E_1\rangle$	$\|13\ E_3\rangle$	$\|22\ G\rangle$
	1471.55	1454.59	1454.80	1456.20
6_4	$\|4\ A_4\rangle$	$\|10\ E_2\rangle$	$\|9\ E_4\rangle$	$\|23\ G\rangle$
	1485.28	1458.53	1458.18	1476.53
6_5	$\|8\ A_1\rangle$	$\|15\ E_1\rangle$	$\|15\ E_3\rangle$	$\|26\ G\rangle$
	1540.67	1535.65	1535.57	1538.11
7_1	$\|6\ A_3\rangle$	$\|11\ E_2\rangle$	$\|14\ E_3\rangle$	$\|25\ G\rangle$
	1560.73	1493.75	1485.91	1492.86
7_2	$\|6\ A_2\rangle$	$\|14\ E_1\rangle$	$\|11\ E_4\rangle$	$\|27\ G\rangle$
	1561.22	1489 94	1495.67	1560.98
a)	$\|5\ A_4\rangle$	$\|12\ E_2\rangle$	$\|12\ E_4\rangle$	$\|28\ G\rangle$
	1592.69	1595.66	1595.85	1593.71
	$\|9\ A_1\rangle$	$\|16\ E_1\rangle$	$\|16\ E_3\rangle$	$\|29\ G\rangle$
	1603.55	1622.48	1621.13	1609.59
	$\|7\ A_3\rangle$	$\|13\ E_2\rangle$	$\|17\ E_3\rangle$	$\|30\ G\rangle$
	1610.32	1628.97	1681.64	1610.60
	$\|7\ A_2\rangle$	$\|17\ E_1\rangle$	$\|13\ E_4\rangle$	$\|31\ G\rangle$
	1610.86	1696.59	1630.34	1627.14

[a] 4 more levels are calculated for every Γ block, but because of the polyad mixing it is no longer possible to indicate their N_K character (first column). The first two rows contain the levels indicated as 7_3 and 7_4 in table 3.

Analysis of the eigenvectors of the total Hamiltonian (eq. (2.1)) shows that the peaks at 708.5 and 728.4 cm^{-1} correspond to transitions to the levels 5_2; these 5_2 levels are split by 19.9 cm^{-1} due to tunneling (table 3). Thus, tunneling effects become visible if the levels approach or exceed the torsional barrier. In our fitting program tunneling is taken into account. For low lying levels tunneling splitting becomes negligible compared to our resolution of about 1 cm^{-1}.

In the measured spectrum there are some unassigned features. In the following we are going to speculate about their possible origins. The fact that we cannot present a definite argument, in the end, does not affect the fit discussed as the main result of this paper. In addition one has to keep in mind that we deal with very weak Raman transitions altogether. Therefore, small concentrations of impurities with strong Raman transitions readily produce spurious transitions.

In our analysis we have not taken into account a coupling between the C-C-C bending mode (A_1-symmetry) and the torsional motion. This coupling arises from mutual hindrance of the CH_3 rotations which diminishes if the C-C-C bending angle opens up for certain positions of the CH_3 tops. This coupling affects only members of the polyads which *a*) possess A_1 symmetry and *b*) are energetically nearly degenerate with the ν_9 levels. The main candidate to be influenced by this coupling seems to be the $2_1(A_1)$-level about 50 cm^{-1} above the first excited ν_9 level.

If we search for effects of this kind in figs. 3a and b, we see that the calculated transition $2_1 \rightarrow 6_1$ at 703.3 cm^{-1} might show a red-shifted component, which could explain the observed peak at 693.7 cm^{-1}. However, this transition is not of A_1 symmetry and therefore we can disregard this idea to explain either of the two unassigned lines at 693.7 cm^{-1} and 748.6 cm^{-1}.

Coupling between the bending mode and torsional motion may result also in the observation of combination bands like $0_1 \rightarrow \nu_9 + 2_1$. This hypothesis does not work either; torsional Raman transitions (between levels of A_1 symmetry) should reappear shifted to the blue by about 369 cm^{-1}. Actually, a number of transitions has been observed shifted by nearly 369 cm^{-1}. Since the observed transitions are not all between levels of A_1 symmetry, we disregard this hypothesis as well.

However, not only Fermi-resonance-like coupling may lead to observable combination bands. Remember that intensities for Raman transitions were derived from a very simple *Ansatz*, $\alpha = \text{const.}\ (\cos 3\alpha_1 + \cos 3\alpha_2)$, eq. (2.8). The constant factor in front of the bracket may be thought of as a first term of a series expansion. A (smaller) term proportional to $q_9(\cos 3\alpha_1 + \cos 3\alpha_2)$ will appear in that same series, which will produce combination tone transitions for each symmetry of the torsional levels concerned. Here, q_9 stands for the normal coordinate of the C-C-C bending motion (A_1 symmetry). These combination bands either yield Raman signals at the position of hitherto unassigned Raman peaks or find an "excuse" like being under a strong plasma line or drowned in a strong background. In two

cases shoulders of nearby Raman transitions may indicate their presence. The transition at 736 cm^{-1} has been remeasured with the Ar^+ 514 nm transition in order to avoid coincidence with the plasma line. In these measurements a weak separate peak has been observed. As to the intensity of these combination bands, note that the observations concern intensities approximately a factor of 100 weaker than strong two-photon transitions. Thus we have presented a possible assignment for the peaks at 693.7 and 748.6 cm^{-1}.

As the only clearly determined impurity of our gas sample we identified iso-butane. Gas-chromatographic measurements yielded a concentration of about 0.1% of this impurity in propane. The Raman spectrum of iso-butane possesses an extremely strong transition (ν_7) at 799 cm^{-1}, which has been observed on the red flank of the ν_8 fundamental of propane at 867 cm^{-1}. The iso-butane signal was found to be 200 times weaker than this ν_8 transition. In addition, a 20 times weaker iso-butane signal at 433 cm^{-1} (ν_8 mode). Both these observations agree with an iso-butane concentration of $0.1 - 0.5\%$.

2.5 A qualitative approach to the torsional spectra

2.5.1 General remarks

Recently a qualitative approach to treat the polyadic rotational and vibrational spectra was proposed based on the analysis of the classical Hamiltonian function corresponding to the effective Hamiltonian for a polyad [13]. It permits to predict and to explain the main features of the polyads such as the existence of regular sequences of levels within the polyads and the quasi-degeneracies of levels forming these sequences. Moreover, it permits to localize the positions of these regular sequences of levels within polyads.

This approach also predicts that with energy increase the polyads will typically undergo qualitative changes (rearrangements), and relates these changes to certain bifurcations in the corresponding classical problem. A well known example of such rearrangements is e.g. the transition from the normal to the local modes in the overtone stretching spectra of molecules containing several bonds.

Here we use this qualitative approach to treat the torsional Raman spectra of propane. In this case we deal with two tops and high barriers for internal rotation and it is possible to neglect the effect of the tunneling splitting of the torsional levels below the barrier, which reduces the problem to the usual vibrational one treated in [13].

2.5.2 Application to propane

First, we neglect tunneling and approximate the potential (eq. (2.2)) by its Taylor series around the potential minimum at $\alpha_1 = \alpha_2 = 0$, truncated at the 4th order terms. This

leads to a potential for two coupled anharmonic oscillators

$$V(\alpha_1,\alpha_2) = a_1(\alpha_1^2+\alpha_2^2) + a_2\alpha_1\alpha_2 + a_3(\alpha_1^4+\alpha_2^4) + a_4(\alpha_1^2+\alpha_2^2)\alpha_1\alpha_2 + a_5\alpha_1^2\alpha_2^2 \qquad (2.11)$$

where the parameters a_n are related to those in eq. (2.2) by

$$\begin{aligned} a_1 &= \tfrac{9}{4}(V_3+4V_6+V_+ +V_-) = 2801.7 \text{ cm}^{-1} \\ a_2 &= \tfrac{9}{2}(V_+ - V_-) = -461.7 \text{ cm}^{-1} \\ a_3 &= -\tfrac{27}{16}(V_3+16V_6+V_+ +V_-) = -2484.0 \text{ cm}^{-1} \\ a_4 &= -\tfrac{27}{4}(V_+ - V_-) = 692.6 \text{ cm}^{-1} \\ a_5 &= -\tfrac{27}{4}(V_+ + V_-) = 1238.0 \text{ cm}^{-1} \end{aligned} \qquad (2.12)$$

The numerical values correspond to the case of propane if we utilize the parameters of table 4. To simplify the application of the theory we introduce new variables

$$Q_k = \left(\frac{a_1}{F}\right)^{1/4} \alpha_k, \quad \hat{P}_k = \left(\frac{F}{a_1}\right)^{1/4} \hat{P}_{\alpha_k} \qquad (2.13)$$

and we rewrite the truncated torsional Hamiltonian in the form

$$\frac{\hat{H}}{2\sqrt{F}\,a_1} = \tfrac{1}{2}(\hat{P}_1^2+\hat{P}_2^2+Q_1^2+Q_2^2) + A\hat{P}_1\hat{P}_2 + BQ_1Q_2 + E(Q_1^4+Q_2^4) + G(Q_1^2+Q_2^2)Q_1Q_2 + UQ_1^2Q_2^2 \qquad (2.14)$$

well suited for further qualitative analysis. Here, for convenience's sake, we have used the same notation for the coefficients as in [13]. One finds

$$\begin{aligned} A &= \frac{1}{2}\frac{F'}{F} = -0.138 \\ B &= \frac{1}{2}\frac{a_2}{a_1} = -0.082 \\ E &= \frac{1}{2}\frac{a_3}{a_1}\sqrt{\frac{F}{a_1}} = -0.020 \\ G &= \frac{1}{2}\frac{a_4}{a_1}\sqrt{\frac{F}{a_1}} = 0.0056 \\ U &= \frac{1}{2}\frac{a_5}{a_1}\sqrt{\frac{F}{a_1}} = 0.010 \end{aligned} \qquad (2.15)$$

Neglecting interaction between the torsional polyads (TPs), we construct an effective Hamiltonian ($\hat{H}_{eff}$). The way to do this is well established. First, we have to rewrite expression (14) for the total Hamiltonian in terms of operators $a_k^\dagger$, a_k (k=1,2) defined by

$$\begin{aligned} Q_k &= (a_k^\dagger + a_k)/\sqrt{2} \\ P_k &= \imath(a_k^\dagger - a_k)/\sqrt{2} \end{aligned} \qquad (2.16)$$

The Hamiltonian thus obtained must be transformed using the well-known canonical transformation techniques. Taking into account only the N-conserving contributions from the different terms in eq. (2.14) we arrive [13] at the following expression for $\hat{H}_{eff}$

$$\frac{\hat{H}_{eff}}{2\sqrt{F}a_1} = \hat{H}_0 + (s_1 + \tfrac{1}{2}s_2)\hat{J}_x + s_2\hat{J}\hat{J}_x + t\hat{J}_x^2 + u\hat{J}_z^2 \tag{2.17}$$

where

$$\begin{aligned} s_1 &= A + B = -0.220 \\ s_2 &= 3G = 0.017 \\ t &= U = 0.010 \\ u &= (6E - U)/2 = -0.065 \end{aligned} \tag{2.18}$$

$\hat{J}_x$, $\hat{J}_z$ and $\hat{J}$ are the Schwinger pseudomomentum operators defined by

$$\begin{aligned} \hat{J}_x &= (a_1^\dagger a_2 + a_2^\dagger a_1)/2 \\ \hat{J}_z &= (a_1^\dagger a_1 - a_2^\dagger a_2)/2 \\ \hat{J} &= (a_1^\dagger a_1 + a_2^\dagger a_2)/2 \end{aligned} \tag{2.19}$$

and $\hat{H}_0$ contains all (irrelevant) terms which are constant within TPs.

The second step consists of the construction of the classical limit to the problem determined by $\hat{H}_{eff}$. For our case this can be done simply by replacing the quantum operators of the pseudomomenta by their quasi-classical counterparts according to

$$\begin{aligned} \hat{J}_x &\rightarrow L\cos\phi\sin\theta \\ \hat{J}_z &\rightarrow L\cos\theta \end{aligned} \tag{2.20}$$

where, as usual, the length $L = J + \frac{1}{2}$ of the classical pseudomomentum is related to N by $N = 2L$ [13].

Omitting $\hat{H}_0$, which is unimportant for our purpose, we can write the expression for H_{cl} in the form

$$\frac{H_{cl}}{2\sqrt{F}a_1} = (s_1 + s_2L)L\cos\phi\sin\theta + tL^2\cos^2\phi\sin^2\theta + uL^2\cos^2\theta \tag{2.21}$$

As a third step we have to find all stable stationary points of the classical Hamiltonian function H_{cl} obtained in the second step and to investigate their behaviour with increasing N. To understand our interest in stationary points of H_{cl} it should be noted that in classical mechanics each stationary point (maximum and minimum) is surrounded by trajectories localized in its vicinity. Under certain conditions, regular (almost harmonic) sequences of quantum states corresponding to these localized trajectories exist. Thus the information

about the stationary points of H_{cl} gives information concerning the existence, the positions and the characteristics (e.g. quasidegeneracies) of the regular sequences of levels in polyads.

In general four types of stationary points are possible. These are listed in table 1 of [13] together with the corresponding values of H_{cl}. An energy increase corresponds to an increase of L or N. The number and the nature of the stationary points of H_{cl} can change as L passes through certain special values. It is this process (called bifurcation) which is responsible for the rearrangements of the TPs with increasing energy.

Using the theory developed in [13] we see that in our case there are two bifurcation points, at $L = L_1^* = 1.32$ and $L = L_2^* = 6.01$. The second bifurcation point, L_2^*, corresponds to energy values high above the potential barrier and thus it has no physical meaning. The value $L_1^* = 1.23$ corresponds to $N = 2.46$, i.e. it corresponds to an energy lying between the third and fourth TP. This energy region is below the potential barrier and is in the domain of validity of H_{eff} (eq. (17)). Thus, the bifurcation point L_1^* has a real physical significance. Below this point (for $L < L_1^*$) the TPs are described by the classical Hamiltonian function H_{cl} with two non-degenerate stationary points corresponding to the top and to the bottom of a given TP. In this case the TPs must be of normal type with approximately equidistant level spacings at their top and bottom. For $L > L_1^*$ the minimum of H_{cl} splits into two degenerate minima and one saddle point. The appearance of two degenerate minima gives rise to the formation of the sequence of quasi-degenerate pairs of levels at the bottom of a TP. Note that the structure at the top of the TP does not change.

Thus we see that our qualitative treatment predicts that the higher TPs in propane will show mixed character: the bottom will be described by the local mode model and the top by the normal mode model. The lower TPs have only normal mode character. The transition from the normal mode to the mixed character takes place already in the fourth TP (see fig. 1). This is the first time that torsional levels have been approximated by an anharmonic oscillator model and treated with this method.

Acknowledgements

We thank J.M. Fernandez-Sanchez and W.L. Meerts for their stimulating interest, especially at the beginning of the experiment, C. Sikkens for technical support, the EEC for a research grant and NWO for financial support

References

[1] P. Groner, J.F. Sullivan and J.R. Durig in *Vibrational Spectra and Structure*, ed. by J.R. Durig, Elsevier, Amsterdam, 1981, volume 9, chapter 6

[2] J.R. Durig, P. Groner and M.G. Griffin, J. Chem. Phys. **66** (1977), 3061

[3] R. Fantoni, K. van Helvoort, W. Knippers and J. Reuss, Chem. Phys. **110** (1986), 1

[4] K. van Helvoort, R. Fantoni, W. Leo Meerts and J. Reuss, Chem. Phys. Lett. **128** (1986), 494

[5] K. van Helvoort, W. Knippers, R. Fantoni and S. Stolte, Chem. Phys. **111** (1987), 445

[6] G. Luyks, J. Timmermans, S. Stolte and J. Reuss, J. Chem. Phys. **77** (1983), 169

[7] G. Luyks, Ph.D. Thesis, Nijmegen, 1983

[8] L. Minnhagen, Arkiv Physik **25** (1963) 203

[9] P.R. Bunker, *Molecular Symmetry*, Academic Press, New York, 1979

[10] Yves G. Smeyers, J. Mol. Struct. **107** (1984), 3

[11] A. Trinkhaus, H. Dreizler and H.D. Rudolf, Z. Naturforsch. **28a** (1973), 750

[12] G. Placzek, in *Handbuch der Radiologie*, ed. by E. Marx, Akademische Verlag, Leipzig, 1934, volume 6, part 2

[13] V.B. Pavlov-Verevkin and B.I. Zhilinskii, Chem. Phys. **128** (1988) 429

Chapter 3

Internal motion of two-top molecules: dimethylamine and propane

R. Engeln, J. Reuss
Department of Molecular and Laser Physics, University of Nijmegen
Toernooiveld, 6525 ED Nijmegen, The Netherlands

D. Consalvo
Dipartimento di Chimica, Universitá "La Sapienza"
P.le A. Moro 5, 00185 Roma, Italy

J.W.I. van Bladel and A. van der Avoird
Department of Theoretical Chemistry, University of Nijmegen
Toernooiveld, 6525 ED Nijmegen, The Netherlands

Abstract

Two molecules with two internal rotors each (CH_3-group) were investigated by spontaneous Raman scattering. The torsional (overtone-) spectra yielded the relevant potential parameters for the internal motions. The potentials show characteristic differences due to the C_{2v} symmetry of propane and C_s symmetry of dimethylamine.

3.1 Introduction

At first glance, the two molecules in the title appear to be similar They possess two methyl groups which can perform torsional motions around their symmetry axes However, the symmetry of the molecules and the potential describing the internal motions are very different Dimethylamine (DMA) can be thought of as an ammonia molecule with two hydrogen atoms replaced by CH_3-groups The molecular symmetry group of DMA is G_{18} The C-N-C plane does not contain the amino-hydrogen H_a [1], this H_a can tunnel between two equivalent positions (an effect not considered in the present work) Propane (PRO) is much more symmetric (molecular symmetry group G_{36}), the two hydrogen atoms of the CH_2 group are placed symmetrically with respect to the C-C-C plane, consequently, fewer potential terms are needed to describe the motion of the two internal rotors [2]

It is customary (though not always sufficient, for certain degenerate irreducible representations of the appropriate molecular symmetry group) to distinguish between two twisting motions of the two CH_3 groups, the libration where both rotate to and fro in the same sense, l_1, the gearing motion, and their libration in the opposite sense, l_2, the anti-gearing motion For PRO, only overtone excitation of these twisting modes is Raman active, whereas for DMA the l_1 libration is also Raman active for an excitation by a single torsional quantum

The experimental apparatus consists of a very sensitive Raman spectrometer, an intracavity set-up with a signal gain of more than a factor 80 with respect to conventional extracavity measurements [2] The achieved optimum resolution is 0 7 cm^{-1} FWHM for strong Raman transitions

There exists much information on torsional spectra for molecules with two internal rotors

Table 1 Torsional potential constants and kinetic coefficients (cm^{-1}) V_3' is put equal to zero (see text)

	PRO		DMA	
	value	error	value	error
V_3	1353	2	1348	2
V_6	18 9	0 5	-7 4	0 7
V_+	-143	2	-122	3
V_-	-40 4	0 8	-128	3
V_3'	–	–	0	
V_6'	–	–	106	1
V_-'	–	–	-364	3
F	5 72	0 01	6 69	0 02
F'	-1 58	0 02	-0 78	0 04

Especially the group of Durig has pioneered the field, employing a Raman spectrometer too [3].The progress reported here comes mainly from the significantly improved sensitivity which allows the observation of transitions between levels where the upper one is near to the barrier hindering free rotation of the internal top. In this way, correlation effects between various potential parameters can be suppressed and the mutual interaction of the two tops can be discussed. Correlation between potential parameters occur when the experimental data are fitted, for low excitation energies, to the model Hamiltonian [4].

3.2 Theoretical aspects

The Hamiltonian is discussed for a non-rotating molecular frame, neglecting the tunnelling (inversion) motion of the H_a of DMA. The kinetic energy terms are given in [2]; the potential energy contribution is

$$\begin{aligned} V(\alpha_1,\alpha_2) \;=\; & \sum_{k=1,2}\Big[\tfrac{1}{2}V_3(1-\cos 3\alpha_k)+\tfrac{1}{2}(-)^{k-1}V_3'\sin 3\alpha_k \\ & +\tfrac{1}{2}V_6(1-\cos 6\alpha_k)+\tfrac{1}{2}(-)^{k}\ {}^{1}V_6'\sin 6\alpha_k\Big] \\ & +\tfrac{1}{2}V_+\big(1-\cos(3\alpha_1+3\alpha_2)\big)+\tfrac{1}{2}V_-\big(1-\cos(3\alpha_1-3\alpha_2)\big) \\ & +\tfrac{1}{2}V_-'\sin(3\alpha_1-3\alpha_2). \end{aligned} \tag{3.1}$$

Here α_k stands for the twisting angle of the k^{th} rotor, $k=1,2$. V_3 is the parameter that mainly determines the barrier of a single top. V_6 influences the width of the barrier. V_+ and V_- suffice to describe the rotor-rotor interaction in case of PRO. V_- (V_+) occurs as a factor of a cosine term which stays constant for the libration l_2 (l_1). (Note that these correspondences are due to the convention of sense of rotation, for the twisting angles α_k).

In eq. (3.1), the terms with V_-' and V_6' vanish for PRO; in case of DMA, however, they are of considerable influence (see table 1). As discussed in the introduction, their origin lies in the fact that the amino hydrogen is positioned out of the C-N-C plane. The parameter V_3' has been put equal to zero, by an appropriate choice of the configuration at which $\alpha_1=\alpha_2=0$ [4].

3.3 Results and discussion

The measured lines we found for PRO and DMA, together with an indication of their experimental strength and their assignment are shown in tables 2 and 3, respectively. N' (N'') stands for the number of torsional (librational) quanta present in the final (initial) state. $\Delta N=1,2$ or 4 denotes the number of quanta absorbed in the Raman transition. For PRO only overtones can be observed, $\Delta N=2$ and 4. Those $N+1$ levels belonging to a fixed number N are said to belong to the same polyad; they are split by the interaction between

the two tops. The subscript K ($N'_{K'}$, $N''_{K''}$) labels the different levels of each polyad. If the symmetry species is shown, (e.g. $N'(G)$) the transitions are resolved, for a defined symmetry type.

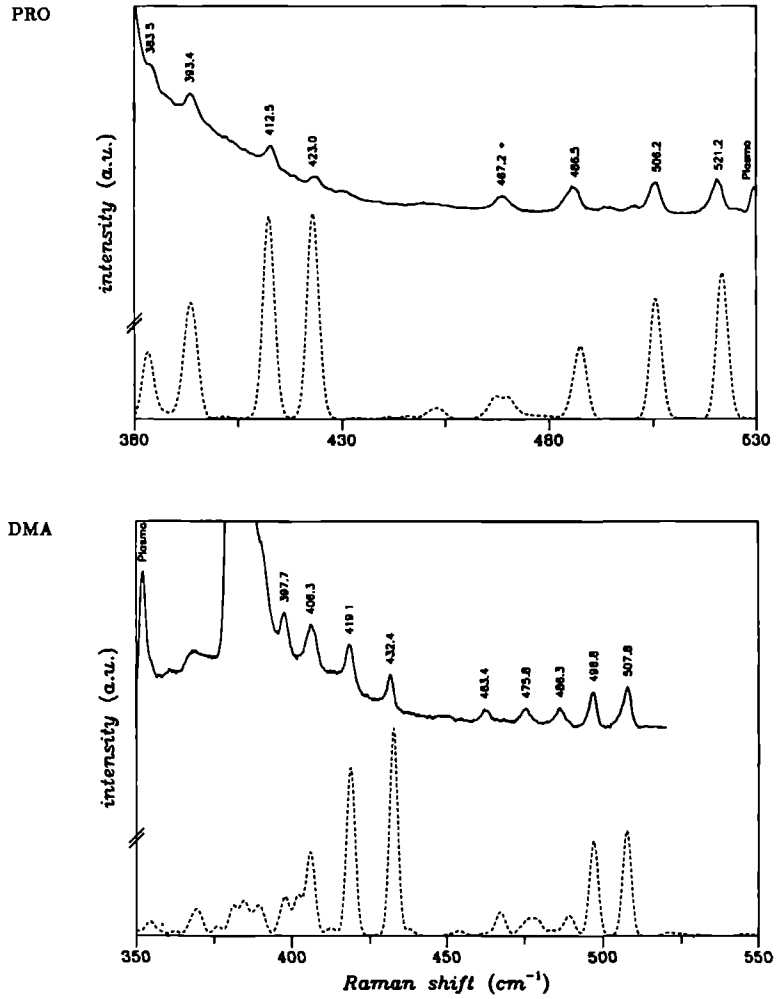

Figure 1: $\Delta N = 2$ torsional overtone spectra for PRO and DMA. The calculated spectra are shown by dashed lines. In the DMA spectrum the strong peak at 384.4 cm^{-1} corresponds to the C-N-C bending mode (ν_{12}).

Table 2: Observed and calculated frequencies and intensities of torsional Raman overtone transitions of propane (cm^{-1})

observed Raman shift	observed relative intensity[1]	assignment $N''_{K''} \rightarrow N'_{K'}$	calculated Raman shift
369.6(1)	–	ν_9, CCC–bend	–
383.5(3)	sh	$1_2 \rightarrow 3_2$	383.23
393.4(2)	s	$2_1 \rightarrow 4_1$	393.58
412.5(1)	s	$1_1 \rightarrow 3_1$	412.39
423.0(1)	m	$0_1 \rightarrow 2_1$	423.05
467.2(2)	s	$2_2 \rightarrow 4_4$	468.61
		$3_4 \rightarrow 5_6$	
486.8(2)	vs	$1_1 \rightarrow 3_3$	487.56
		$2_3 \rightarrow 4_5$	
506.2(1)	vs	$1_2 \rightarrow 3_4$	505.62
521.2(1)	vs	$0_1 \rightarrow 2_3$	521.61
686.9(3)	w	$2_3 \rightarrow 6_3(E_1, E_3, G)$	688.19
		$3_1 \rightarrow 7_1(A_3)$	
		$3_1 \rightarrow 7_2(G)$	
693.7(3)	–	–	–
702.8(3)	vw	$2_1 \rightarrow 6_1(E_3)$	703.32
		$2_1 \rightarrow 6_2(G)$	
708.5(3)	vw	$1_2 \rightarrow 5_2(E_1, E_4)$	708.21
		$2_1 \rightarrow 6_1(E_1)$	
718.8(3)	vw	$3_2 \rightarrow 7_4(A_2)$	716.56
		$3_2 \rightarrow 7_3(G)$	
		$2_3 \rightarrow 7_1(E_3)^2$	
728.4(3)	vw	$1_2 \rightarrow 5_2(A_2, G)$	728.82
736.0(5)	–	–	–
748.6(3)	–	–	–
758.6(3)	vw	$1_1 \rightarrow 5_1(E_2, E_3, G)$	758.92

1 vs = very strong, s = strong, m = medium, w = weak, vw = very weak, sh = shoulder.

2. The label 7_1 indicates a strongly mixed polyad level, with a strong admixture of the $N' = 6$ polyad.

Table 3: Observed and calculated frequencies and intensities of torsional Raman transitions of dimethylamine (cm^{-1})

observed Raman shift	observed relative intensity[1]	assignment $N''_{K''} \rightarrow N'_{K'}$	calculated Raman shift
176.6(7)	vvw	$1_2 \rightarrow 2_1$	176.93
235.2(4)	vw		
239.7(4)	vw		
243.2(7)	vw	$1_1 \rightarrow 2_2$	243.60
250.2(4)	w	$1_2 \rightarrow 2_3$	251.90
256.3(4)	w	$0_1 \rightarrow 1_2$	255.66
311.7(4)	w		
384.4(1)		ν_{12}, CNC-bend	
385.5(5)	sh		
390.7(4)	m	$3_1 \rightarrow 5_2$ (E_1, E_2)	390.73
397.7(2)	m	$2_1 \rightarrow 4_1$	397.95
406.4(2)	s	$1_2 \rightarrow 3_2$	406.11
419.1(2)	s	$1_1 \rightarrow 3_1$	418.92
432.4(2)	s	$0_1 \rightarrow 2_1$	432.59
463.2(3)	m	$2_1 \rightarrow 4_3$	463.52
475.8(3)	m	$2_2 \rightarrow 4_4$	474.61
486.3(2)	s	$1_1 \rightarrow 3_3$	486.62
496.8(2)	s	$1_2 \rightarrow 3_4$	497.04
507.8(2)	s	$0_1 \rightarrow 2_3$	507.56

1. s = strong, m = medium, w = weak, vw = very weak, vvw = very very weak, sh = shoulder.

In general the mutual top interaction mixes the states within a polyad, for instance 3 quanta in one rotor, 0 in the other one, (3,0), with (2,1), (1,2) and (0,3). Where the mixing is minimal, the transitions are stronger, since then the overlap between initial and final wavefunction is maximal.

For PRO this maximum overlap occurs for "vertical" transitions between levels of polyads either with the lowest possible values of the K-subscript or with the highest ones. Consequently, two series of strong $\Delta N = 2$ overtones (see fig. 1) are observed. For DMA there are more interaction terms in the potential leading to a more mixed situation [4]. The Raman intensity is spread out over more and weaker transitions and therefore the $\Delta N = 4$ ones become unobservable. However, as discussed in the introduction, $\Delta N = 1$ transitions

become Raman allowed so that a sufficient number of lines could be measured to achieve a satisfactory determination of the potential parameters in eq. (3.1) [5].

In table 1 these potential parameters are listed both for PRO and DMA. The potential barrier is comparable for both molecules. For DMA the mutual two-top potential (characterized by the parameters V_+, V_- and V'_-) produce significant changes, especially through the term with V'_-, which is absent in case of propane. Remember, that from our measurements we cannot deduce how the one-top-minimum geometry $\alpha_1 = \alpha_2 = 0$ actually looks. The V_+ and V_- and V'_--terms drive the real minimum towards $\alpha_1 = -\alpha_2 = 2.8°$. In addition, for the reflection $\alpha_1 \rightleftharpoons \alpha_2$ the potential becomes very asymmetric, see fig. 2.

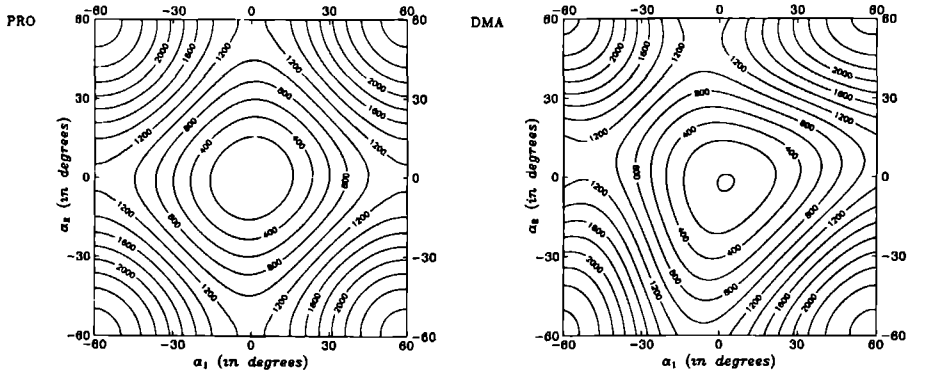

Firgure 2: Torsional potential for PRO and DMA. The numbers indicating the contour lines are energy values in wavenumbers.

In case of DMA the relatively large value of F is a consequence of kinetic correction [6]. These corrections add to the value of the rotational constant of a methyl group, rotating around its symmetry axis. Without kinetic corrections, for a rigid CH_3-rotor the values 5.3 and 5.2 cm^{-1} are calculated for these rotational constants of DMA and PRO, respectively. The values F and F' (table 1) are obtained through a fit of the Hamiltonian to our experimental results.

References

[1] J.E. Wollrab and V.W. Laurie, J. Chem. Phys. **48** (1978),5058

[2] R. Engeln, J. Reuss, D. Consalvo, J.W.I. van Bladel, A. van der Avoird and V. Pavlov-Verevkin, Chem. Phys. **144** (1990) 81

[3] P. Groner, J.F. Sullivan and J.R. Durig, *Vibrational Spectra and Structure* , vol 9, Elsevier, Amsterdam, 1981

[4] P. Groner and J.R. Durig, J. Chem. Phys. **66** (1977), 1856

[5] R. Engeln, J. Reuss, D. Consalvo, J.W.I. van Bladel and A. van der Avoird (in preparation).

[6] A. Trinkhaus, H. Dreizler and H.D. Rudolf, Z. Naturforsch. **28a** (1973), 750

Chapter 4

Methyl torsion in $C_2H_{4-n}(CH_3)_n$, n = 1&2

R. Engeln and J. Reuss
Department of Molecular and Laser Physics, University of Nijmegen,
Toernooiveld, 6525 ED Nijmegen, The Netherlands

Abstract

Torsional Raman spectra of trans-2-butene, cis-2-butene, 2-methylpropene and propene are recorded. The molecular parameters describing the torsional motions are determined. Especially, the torsional barrier parameters, V_3, and the reduced moments of inertia, F, of the tops are compared with the values determined from MW-data. We conclude that one has to analyse together MW- and Raman data in order to obtain a reliable description of internal motions.

4.1 Introduction

Molecules with internal torsional degrees of freedom have been mainly studied by high resolution microwave spectroscopy [1, 2, 3, 4] and by low resolution Raman (overtone) scattering, sometimes flanked by IR absorption measurements [5, 6, 7]. The drawback of the Raman method that rotation is not resolved is compensated by the fact that high torsional levels even above the torsional barrier can be accessed.

In principle, the quantum-mechanics of compounds with one and two methylic rotors is well understood; their analysis is based on a hamiltonian derived by Herschbach as early as 1956 [8]. However, the values of the parameters occuring in the hamiltonian, especially those describing the mutual interaction of two methyl groups, were badly known. For propane and dimethylamine we recently were able to determine these parameters [9, 10]. Here we will present experimental results on a family of related molecules in order to investigate the influence of the changing configurations on the potential parameters. We have chosen ethene as basic molecule (see fig. 1), replacing two hydrogen atoms by CH_3-groups yielding cis- and trans-2-butene and 2-methylpropene (isobutene). For comparison, propene $(CH_3)HC{=}CH_2$ has also been measured. Our technique is sensitive spontaneous intracavity

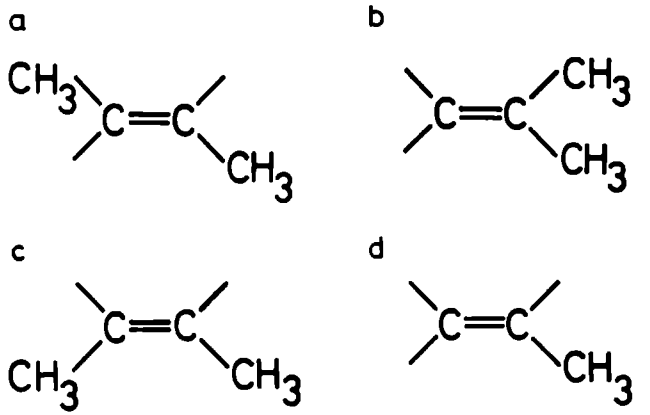

Figure 1: Structural representation of trans-2-butene (a), 2-methylpropene (b), cis-2-butene (c) and propene (d)

Raman scattering as applied in [9, 10].

The literature contained some surprises (see table 1); we started with the conviction that the barrier parameter, V_3, would be nearly the same for the four compounds and that the

other parameters, notably V_+ and V_- describing the mutual interaction of the CH_3-groups, would differ greatly. However, cis-2-butene has been reported to posses a V_3-value three times smaller than that of 2-methylpropene [5, 6]. This fact made a new measurement even more attractive.

Table 1: Comparison of V_3-values and torsional barrier heights (BH) determined from MW-data and IR/Raman-data (values in cm^{-1}). Note, that the V_3-value from MW-measurements stands for an effective $V_{3,MW} = V_3 + 4V_6 + V_+ + V_-$.

'one-CH_3-top' molecules			'two-CH_3-top' molecules			
	$(CH_3)CH_3$ ethane			$(CH_3)CH_2(CH_3)$ propane		
$V_3 = 1009$	Raman[a]		$V_3 = 1353$	BH = 1170	Raman[c]	F = 5.72
$V_3 = 1012.0$	IR[b]		$V_3 = 1108$		MW[d]	F = 6.13
	$(CD_3)CD_3$					
$V_3 = 990$	Raman[e]	F = 1.3416				
$V_3 = 989$	IR[f]	F = 1.3416				
	$(CH_3)NH_2$ methylamine			$(CH_3)NH(CH_3)$ dimethylamine		
$V_3 = 684.71$	MW[g]	F = 7.1	$V_3 = 1350$	BH = 1096	Raman[h]	F = 6.7
			$V_3 = 1128$		MW[r]	F = 6.49
	$(CH_3)HC{=}O$ acetaldehyde			$(CH_3)_2C{=}O$ acetone		
$V_3 = 406$	MW[i]	F = 7.5	$V_3 = 279.4$		IR[j]	F = 5.73
			$V_3 = 266.3$		MW[k]	F = 5.59
	$(CH_3)CH{=}CH_2$ propene			$(CH_3)HC{=}CH(CH_3)$ trans-2-butene		
$V_3 = 721.3$	Raman[l]	F = 7.1	$V_3 = 712.7$	BH = 712.7	IR&Raman[n]	F = 7.05
$V_3 = 693.7$	IR&Raman[s]	F = 7.1007	$V_3 = 861.1$	BH = 861.1	Raman[l]	F = 4.94
$V_3 = 698.4$	MW[m]	F = 7.1007		iso-butene		
			$V_3 = 893.7$	BH = 728.0	IR&Raman[o]	F = 5.77
			$V_3 = 1079.0$	BH = 974.3	Raman[l]	F = 3.30
			$V_3 = 759.5$		MW[p]	
				cis-2-butene		
			$V_3 = 274.6$	BH = 250.0	IR[n]	F = 5.63
			$V_3 = 261$		MW[q]	F = 5.69

a) ref. [18] *b*) ref. [13] *c*) ref. [9] *d*) ref. [4] *e*) ref. [11] *f*) ref. [14] *g*) ref. [2] *h*) ref. [10] *i*) ref. [15] *j*) ref. [17] *k*) ref. [16] *l*) our result *m*) ref. [1] *n*) ref. [6] *o*) ref. [5] *p*) ref. [19] *q*) ref. [3], recently confirmed by the group of Prof. Dreizler [21] *r*) ref. [22] *s*) ref. [7]

Another point of interest resides in the fact that the determination of barrier parameters from MW- and Raman-data often leads to quite different values, even for well studied species like propane [4]. The present work might help to shed some light upon the problem.

4.2 Experimental

The experimental set-up has already been described in a recent article on the torsional motion of the CH_3-groups of propane [9]. It consists of an Ar^+-laser (Spectra Physics, model 2030-15S) from which the output mirror is removed and replaced by two highly reflecting curved mirrors (R = 50 mm, R = 100 mm), placed adjustably inside the sample cell.

The working pressure for cis- and trans-2-butene was 0.7 bar and for 2-methylpropene 0.9 bar, because at higher pressures small droplets, formed during the measurement, caused severe fluctuations of the laserpower. In the case of propene we worked at a pressure of 1 bar, mainly because the cell was not constructed to stand over-pressure. During the measurements of trans-2-butene and propene a thin film was formed on the (intracavity-)brewster window of the cell, which caused a decrease of laserpower by more than 50%. In both cases the window could be cleaned by using methanol; in the case of trans-2-butene it had to be done every day, in the case of propene every three days. All gases were purchased from Intermar b.v., with 99.0% purity.

Due to a change in laser tube and brewster window a factor of 1 5 is gained in laserpower, compared to our propane measurements [9]. An intracavity power of 450 Watts is achieved for the 514.5 nm laser line. Some measurements are performed with the 488 nm laser line in order to avoid overlap of a strong plasma line with a weak Raman transition The laserpower is stabilized by controlling the light which leaks through the folding mirror (R = 100 mm) of the cavity. This signal is fed back to the power supply, which controls the current of the discharge.

The scattered Raman light, produced in the laserfocus (waist of $2w_0 = 50\ \mu m$), is collected under 90° with respect to the beam propagation and laser polarization. The focus is imaged by an f/8 lens on the entrance slit of a double monochromator (Jobin Yvon Ramanor HG2S). The four slits of this monochromator are all electronically adjustable. The measurements are performed at a resolution of 1.5 cm^{-1} (e.g. 100 μm slitwidth) for the strong transitions and 2 0 cm^{-1} (e.g. 200 μm slitwidth) for the weak transitions.

The light is measured with a cooled RCA C31034-02 photo multiplier (PMT). The output data of the PMT is handled, via a photn counting system (Ortec Brookdeal 5C1), by an Apple IIe computer. This computer also controls the scanning of the gratings of the double monochromator. The frequency is calibrated with the help of several Ar^+-transitions in the discharge inside the lasertube. The accuracy achieved is 0.5 cm^{-1} for the weak transitions and 0 3 cm^{-1} for the strong transitions. The Raman spectra are recorded with typical

scan velocities of 40 cm^{-1}/hour for the strong transitions and 8 cm^{-1}/hour for the weak transitions.

4.3 The Torsional Hamiltonian

4.3.1 'two-top' molecules

The torsional Hamiltonian for the non-rotating cis-2-, trans-2- and isobutene molecule can be written as

$$\hat{H} = F(\hat{P}_{\alpha_1}^2 + \hat{P}_{\alpha_2}^2) + F'\hat{P}_{\alpha_1}\hat{P}_{\alpha_2} + V(\alpha_1, \alpha_2) \quad \alpha_1,\ \alpha_2 \in [-\pi,\ \pi\rangle, \tag{4.1}$$

with the following Fourier expansion, up to sixth order, for the potential

$$\begin{aligned} V(\alpha_1, \alpha_2) \;=\; & \sum_{k-1,2} \left[\tfrac{1}{2}V_3(1 - \cos 3\alpha_k) + \tfrac{1}{2}V_6(1 - \cos 6\alpha_k)\right] \\ & + \tfrac{1}{2}V_+\big(1 - \cos(3\alpha_1 + 3\alpha_2)\big) + \tfrac{1}{2}V_-\big(1 - \cos(3\alpha_1 - 3\alpha_2)\big). \end{aligned} \tag{4.2}$$

The angles α_1 and α_2 describe the torsions about the C–C bonds. The momenta conjugate to the torsional angles are obtained from $\hat{P}_{\alpha_1} = -\imath\frac{\partial}{\partial\alpha_1}$ and $\hat{P}_{\alpha_2} = -\imath\frac{\partial}{\partial\alpha_2}$. The parameters V_3 and V_6 describe the top-frame interaction; V_+ and V_- describe the anti-geared and geared top-top interactions. The coefficients F and F' are determined by the geometrical properties of the molecule [12]. In principle F is the reduced rotational constant of the two tops; F' is a kinetic interaction constant. The barrier height (BH) is defined as the height of a saddle point (transition state) above a local minimum of the two-dimensional potential function; i.e. BH equals $V_3 + V_+ + V_-$.

Our notation for the Hamiltonian (eq. (4.1)) differs somewhat from that used by Durig *et al.* [5, 6]. The correspondence can be expressed by $F = \frac{1}{2}\hbar^2 g^{44} = \frac{1}{2}\hbar^2 g^{55}$, $F' = \hbar^2 g^{45}$, $V_3 = V_{30} = V_{03}$, $V_6 = V_{60} = V_{06}$, $V_+ = \frac{1}{2}(V'_{33} - V_{33})$ and $V_- = -\frac{1}{2}(V'_{33} + V_{33})$.

For the parameters in the Hamiltonian (eq. (4.1)) the fitting procedure has been described in [9]. For the Raman intensities we assumed that the average polarizability has the following dependence on the torsional angles

$$\alpha \propto \cos(3\alpha_1) + \cos(3\alpha_2). \tag{4.3}$$

The labelling of the levels, N_K, is the same as for propane. N denotes the total number of torsional quanta in the molecule, distributed as they might be over the two torsional degrees of freedom. Due to the interaction between the two tops and due to anharmonicity effects every level with the same total number of torsional quanta N, is split into $N + 1$ levels, labelled by K (see fig. 2). In fig. 2 tunneling splitting is neglected. The tunneling is responsible for the splitting of every N_K-level into one non-degenerate (A), two two-fold (E) and one four-fold degenerate (G) level. In view of our limited spectral resolution this splitting is only measurable for levels close to the top of the barrier.

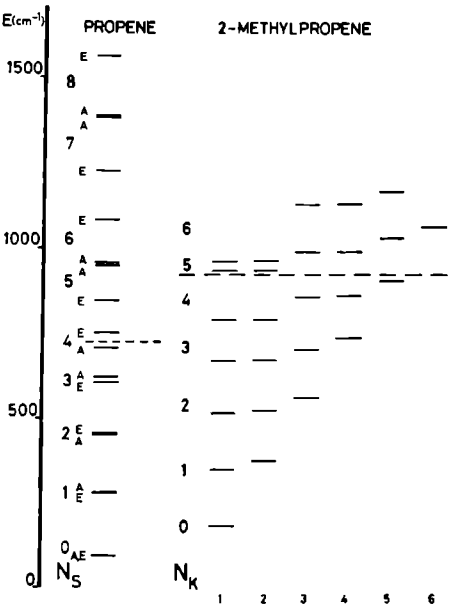

Figure 2: Energy level scheme for propene and 2-methylpropene. In the case of 2-methylpropene only the levels with A symmetry are drawn, thus neglecting tunneling splitting. The dashed lines indicate the height of the torsional potential barrier for one top.

4.3.2 'one-top' molecules

In the case of propene we deal with only one top. This simplifies the expression of the Hamiltonian (eq. (4.1)) in the following way

$$\hat{H} = F\hat{P}_\alpha^2 + V(\alpha) \quad \alpha \in [-\pi, \pi\rangle, \tag{4.4}$$

with

$$V(\alpha) = \tfrac{1}{2}V_3(1 - \cos 3\alpha) + \tfrac{1}{2}V_6(1 - \cos 6\alpha) \tag{4.5}$$

The top-frame interaction terms describe completely the torsional potential.

For the Raman intensities we assumed, similar to the case of the 'two-top' molecules, that the average polarizability has the following dependence on the torsional angle

$$\alpha \propto \cos(3\alpha). \tag{4.6}$$

In propene every level is split into one non-degenerate (A) and one two-fold degenerate

(E) level due to tunneling. The levels are denoted N_A or N_E, in which N is the number of torsional quanta in the top (see fig. 2).

4.4 Results

4.4.1 2-methylpropene

In fig. 3b part of the torsional Raman spectrum of 2-methylpropene is shown. In addition to the 8 Raman transitions mentioned by the group of Durig [5], we measured two new lines which we assign to torsional transitions. Due to a perturbation of the 1_2 torsional level [5], several transitions were not used to determine the parameters which describe the torsional motion (see table 2), because the Hamiltonian (eq. (4.1)) can not handle these perturbations.

If we assume that the 1_2-level is pushed down in energy, this explains why the $1_2 \rightarrow 3_4$ and the $1_2 \rightarrow 2_3$ transitions are shifted to the blue, and the $0_1 \rightarrow 1_2$ transition to the red. In [5] it is discussed as an interaction of a low frequency bending mode (B_2) with the 1_2 torsional level. We included the far infrared measurements of Durig *et al.* [5] in the fit and the parameters we found are shown in table 5.

Table 2: Observed and calculated frequencies of torsional transitions of 2-methylpropene (cm^{-1})

Infrared[a]	assignment	calculated
145.4	$3_1 \rightarrow 4_2$	145.4
158.1	$2_1 \rightarrow 3_1$	157.5
162.5	$1_1 \rightarrow 2_1$	162.8
164.8		
165.0	$0_1 \rightarrow 1_1$	165.3
165.2	$2_1 \rightarrow 3_2$	165.6
175.4		
176.3	$3_4 \rightarrow 4_5$	176.1
181.6	$2_2 \rightarrow 3_3$	179.2
186.0	$2_3 \rightarrow 3_4$	185.1
196.0	$1_2 \rightarrow 2_3^b$	193.0
197.6	$0_1 \rightarrow 1_2^b$	200.0

Raman	assignment	calculated
274.9(3)	$2_3 \rightarrow 4_3$	275.5
293.0(3)	$1_2 \rightarrow 3_2^b$	293.7
319.9(3)	$1_1 \rightarrow 3_1$	320.2
328.9(3)	$0_1 \rightarrow 2_1$	327.9
341.1(3)	$2_1 \rightarrow 4_3$	340.5
360.6(3)	$2_3 \rightarrow 4_5$	361.5
372.2(3)		
380.3(3)	$1_2 \rightarrow 3_4^b$	378.1
382.7(3)		
393.2(3)	$0_1 \rightarrow 2_3$	393.0

[a] from ref. [5]

[b] not used in the fit

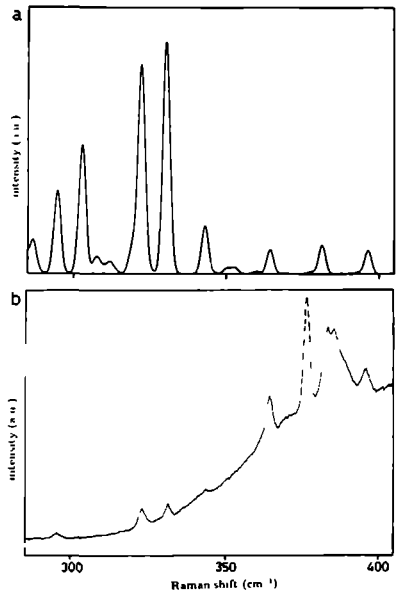

Figure 3: Calculated torsional Raman spectrum (a) and measured Raman spectrum (b) of 2-methylpropene

If we look at the intensities in the calculated spectrum (fig. 3a), we have to keep in mind that we assumed a very simple ansatz for the polarizability, $\alpha \propto \cos(3\alpha_1) + \cos(3\alpha_2)$. From calculations on 1,3-butadiene we know that by adding a second term in the Fourier expansion of α, e.g. const.$(\cos(6\alpha_1) + \cos(6\alpha_2))$, relative intensities can easily change [20].

4.4.2 trans-2-butene

The torsional Raman spectrum was already recorded by the group of Durig [6]. They measured and assigned three Raman and three infrared transitions. Two other weak Raman lines were mentioned but not assigned. We measured the Raman spectrum (fig. 4b) with a different laser line, i.e. 488 nm, and discovered that one of the Raman transitions mentioned in [6] was a plasma line. In addition, we were able to assign the two weak Raman transitions, mentioned by the group of Durig, as torsional transitions.

Together with these four torsional Raman transitions two torsional infrared transitions [6] were used to fit the torsional Hamiltonian (eq. (4.1)). We started with fitting V_3, V_6, F and F' (i.e. we did not rely on calculations of the kinetic coefficient (g^{mn}) using the structure of propene [6]). After this preliminary fit F and F' were taken as constants

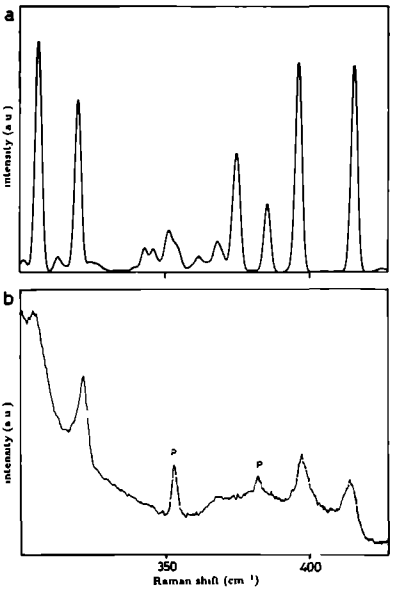

Figure 4: Calculated torsional Raman spectrum (a) and measured Raman spectrum (b) of trans-2-butene. P indicates a plasma line.

and V_+ and V_- were included in the fit. In this way we could not improve the fit, which means that the gearing and antigearing terms of the two tops are not observable within our spectral resolution.

Table 3: Observed and calculated frequencies of torsional transitions of trans-2-butene (cm^{-1}). The Raman-column contains our new results.

Raman	Infrared[a]	assignment[b]	calculated
	163.6	$0_1 \rightarrow 1_1$	163.0
	156.9	$1_1 \rightarrow 2_1$	156.7
305.0(3)		$1_1 \rightarrow 3_1$	306.0
320.0(3)		$0_1 \rightarrow 2_1$	319.6
397.5(3)		$1_2 \rightarrow 3_4$	396.7
415.0(3)		$0_1 \rightarrow 2_3$	415.5

[a] from ref. [6]

[b] the notation is explained in section 4.3

With respect to the parameters values of Durig [6] a barrier height, V_3, was found which is 20% higher and a F value which is 30% lower. Note, that the barrier parameters of table 1, column a have to be considered as effective values because V_+ and V_- are omitted.

4.4.3 cis-2-butene

In the Raman spectrum of cis-2-butene we observed one torsional transition at 202.2 cm^{-1}. This supports the far infrared measurements of Durig [6], who observed a transition at 101.0 cm^{-1} and at 102.2 cm^{-1}. They were assigned to $0_1 \rightarrow 1_2$ and $1_2 \rightarrow 2_3$ transitions, respectively. The values for the parameters of the torsional Hamiltonian (eq. (4.1)) given in table 5 are taken from ref. [6].

The value for the barrier height, V_3, is in good agreement with the value determined from MW-data (see table 1). But also here, the V_3-value is determined omitting V_+ and V_-.

4.4.4 propene

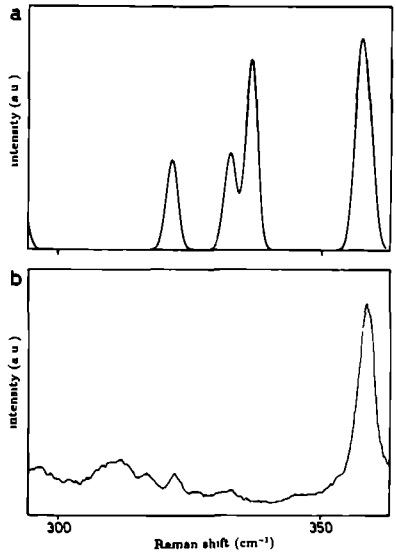

Figure 5: Calculated torsional Raman spectrum (a) and measured Raman spectrum (b) of propene.

Part of the Raman spectrum of propene is shown in fig. 5b. In a slow scan at higher resolution (1.0 cm^{-1}) two peaks were partially resolved round 333 cm^{-1}. The broad feature

at 314 cm^{-1} and the peak at 317.4 cm^{-1} could not be assigned. In the fit F is taken as a constant and put equal to the value used by E. Hirota [1]. The results for V_3, V_6 and F are given in table 5. Our values are in good agreement with the values determined previously [1, 7] (see table 1 and 5).

Table 4: Observed and calculated frequencies of torsional Raman overtone transitions of propene (cm^{-1}).

observed Raman shift	assignment	calculated Raman shift
317.4(3)		
323.3(3)	$1_F \rightarrow 3_E$	321.3
333(1)	$3_A \rightarrow 5_A$	330.8
	$4_E \rightarrow 6_E$	331.7
	$1_A \rightarrow 3_A$	336.1
357.7(3)	$0_A \rightarrow 2_A$	357.6
	$0_E \rightarrow 2_E$	359.4

4.5 Discussion

In this paper we present new experimental Raman results on three related molecules which led to an improved value of the potential parameters (table 5). Especially, for 2-methylpropene (isobutene) a full set of parameters has been derived.

There are two aspects of these data; one is the fact that from high torsional levels (see fig. 2; the highest N_K-value reached by Raman transitions are 4_3 and 4_5, see table 2) we could derive V_+- and V_--constants of eq. (4.2); to put it even stronger, we were forced to include these mutual top-top interactions in order to fit the experimental data. This inclusion has large consequences also for the low lying torsional levels. From the calculations follows that the $N_K = 0_1$ levels assume a tunneling splitting between the $\Gamma = E$ and $\Gamma = G$ level of 2.0 MHz and of 3.9 MHz between $\Gamma = E$ and $\Gamma = A$ level, with the parameters of table 3; if one puts $V_+ = V_- = 0$ one finds, however, 0.45 and 0.93 MHz, respectively. Similarly, one obtains -45 & -93 MHz and 16 & 30 MHz for $N_K = 1_1$ and -72 & -144 MHz and -15 & -30 MHz for $N_K = 1_2$.

To be sure, we were not able to resolve the tunneling splitting of these levels with the here applied spontaneous Raman technique. The point is that for MW-measurements they must be included since there these effects are resolvable, in principle. In practice, comparable splittings (for the low lying levels) can be achieved with effective V_3-values omitting V_-

Table 5: Torsional potential constants and kinetic coefficients (cm^{-1}).

	2-methyl-propene		trans-2-butene		cis-2-butene		propene	
	a)	b)	a)	c)	a)	c)	a)	d)
V_3	1079.0	893.7	861.1	712.7		274.6	721.3	693.7
V_6	124.0	−4.0	17.6	−4.0			−36.2	−14.0
V_+	−354.0	−150.4		−24.2[e]		f)		
V_-	249.3	−15.3		24.2[e]		f)		
F	3.20	5.77	4.94	7.05		5.63	7.1	7.1
F'	1.42	−0.353	−2.56	−3.46		0.11		

[a] our result
[b] ref. [5]
[c] ref. [6]
[d] ref. [7]
[e] $V'_{33} = -48.4$, $V_{33} = 0$
[f] $V_{33} = 24.6$ If we assume $V'_{33} = 0$, $V_+ = -12.3$ & $V_- = -12.3$

and V -interactions. In our view, it is thus very important to analyse together MW- and Raman-data to obtain a reliable and probably very accurate description of internal motions. Notably, in view of the big discrepancies a combined analysis seems necessary for propane and isobutene (see table 1).

The other aspect of the presented data is the large variation of barrier heights for seemingly similar molecules. Here, the strongest surprise comes from cis-butene as compared to trans- and isobutene. The naive expectation is that here the two tops possess an intermediate distance to each other and thus should show an intermediate barrier, whereas the experiments so far yield a barrier three times lower. It is a pity that we were not able to obtain good Raman data on this system to clear the issue whether the low barrier values for cis-butene are a consequence of considering a truncated Hamiltonian.

Table 1 contains similar surprises for other systems. Comparison between acetaldehyde and acetone yields V_3-values differing by a factor 1.5, or even more strikingly, comparison between methylamine and dimethylamine show V_3-values differing by a factor 2.

Whether these extremely big differences are due to that one compares effective values for V_3, is an open question. The comforting fact is that when there are simple systems considered (notably $(CH_3)CH_3$) MW- and Raman measurements lead to satisfying agreement, and whene the same technique is applied to one- and related two-top molecules (notably propene and trans-2-butene) rather consistent and similar barriers are obtained.

Acknowledgements

The authors would like to thank Prof. H. Dreizler for his unpublished results, J. van Bladel for the use of his computer program, C. Sikkens for technical assistance and NWO for financial support.

References

[1] Eizi Hirota. J. Chem. Phys. **45** (1966) 1984

[2] N. Ohashi, S. Tsunekawa, K. Takagi and J.T. Hougen, J. Mol. Spectr. **137** (1989) 33

[3] S. Kondo, Y. Sakurai, E. Hirota and Y. Morino, J. Mol. Spectr. **34** (1970) 231

[4] G. Bestmann, W. Lalowski and H. Dreizler, Z. Naturforsch. **40a** (1985) 271

[5] J.R. Durig, W.J. Natter and P. Groner, J. Chem. Phys. **67** (1977) 4948

[6] J.R. Durig, S.D. Hudson and W.J. Natter. J. Chem. Phys. **70** (1979) 5747

[7] J.R. Durig, G.A. Guirgis and S. Bell, J. Phys. Chem. **93** (1989) 3487

[8] D.R. Herschbach, J. Chem. Phys. **31** (1959) 91

[9] R. Engeln, J. Reuss, D. Consalvo, J.W.I. van Bladel, A. van der Avoird and V. Pavlov-Verevkin, Chem. Phys. **144** (1990) 81

[10] R. Engeln, J. Reuss, D. Consalvo, J.W.I. van Bladel and A. van der Avoird, Chem. Phys. Lett. **170** (1990) 206

[11] J.M. Fernandez-Sanchez, A.G. Valdenebro and S. Montero, J. Chem. Phys. **91** (1989) 3327

[12] A. Trinkaus, H. Dreizler and H.D. Rudolph, Z. Naturforsch. **28a** (1973) 750

[13] N. Moazzen-Ahmadi, H.P. Gush, M. Halpern, H. Jagannath, A. Leung and I. Ozier, J. Chem. Phys. **88** (1988) 563

[14] N. Moazzen-Ahmadi, A.R.W. McKellar, J.W.C. Johns and I. Ozier, to be published

[15] W. Liang, J.G. Baker, E. Herbst, R.A. Booker and F.C. De Lucia, J. Mol. Spect. **120** (1986) 298

[16] J.M. Vacherand, B.P. van Eijck, J. Burie and J. Demaison, J. Mol. Spectr. **118** (1986) 355

[17] P. Groner, G.A. Guirgis and J.R. Durig, J. Chem. Phys. **86** (1987) 565

[18] R. Fantoni, K. van Helvoort, W. Knippers and J. Reuss, Chem. Phys. **110** (1986) 1

[19] J. Demaison and H.D. Rudolph, J. Mol. Struct. **24** (1975) 325

[20] R. Engeln, D. Consalvo and J. Reuss, to be published

[21] H. Dreizler, private communication

[22] J.E. Wollrab and V.W. Laurie, J. Chem. Phys. **54** (1971) 532

Chapter 5

Evidence for a gauche minor-conformer of 1,3-butadiene

R. Engeln, D. Consalvo* and J. Reuss
Department of Molecular and Laser Physics, University of Nijmegen
Toernooiveld, 6525 ED Nijmegen, The Netherlands

* Dipartimento di Chimica Università "La Sapienza",
P. le A. Moro 5, 00185 Rome, Italy

Abstract

We present experimental Raman data on torsional transitions that prove that the less stable conformer of 1,3-butadiene has a gauche structure. It is shown that in order to predict the relative intensities of the 'gauche' transitions with respect to the 'trans' transitions, one has to include a second order term in the Fourier expansion of the molecular polarizability.

5.1 Introduction

It is well known that the more stable rotamer of 1,3 butadiene possesses planar trans geometry [1, 2] (see fig. 1). Theoretical and experimental attempts to establish the structure of the less stable conformer led to contradictory results. In 1970 ab initio calculations of Radom and Pople [3] suggested that the minor conformer had a planar cis structure (see fig. 1). In 1976 Skaarup *et al.* [4] pointed out that the gauche structure was energetically lower than the cis. However, the difference was only 0.6 kcal/mol (210 cm ^{1}) which they did not consider to be conclusive. Eight years later Breulet *et al.* [5] calculated the gauche form to be 0.7 kcal/mol (245 cm ^{1}) more stable than the cis, but in 1985 Feller and Davidson [6] concluded that theory could not decide unambiguously which of the two form had a lower energy. From the experimental point of view direct measurements to exclude one of the two geometries are difficult. At room temperature only 1% of the minor form is present according to an estimate of the Boltzmann distribution assuming a reasonable torsional potential. On the basis of NMR spectroscopy Lipnick and Garbisch [7] are in favour of the gauche 1,3-butadiene as the second stable conformer. On the contrary IR- and UV-absorption spectra of matrix-isolated 1,3-butadiene yield the cis structure for the minor conformer [8, 9, 10]. The question thus remains whether the structure for the minor conformer is cis or gauche. A very recent study addresses properly the question of the structure of the less stable isomer of butadiene [11]. The conclusion of this paper is in favour of a gauche second conformer geometry according to ab initio calculations, vibrational and electronic absorption data.

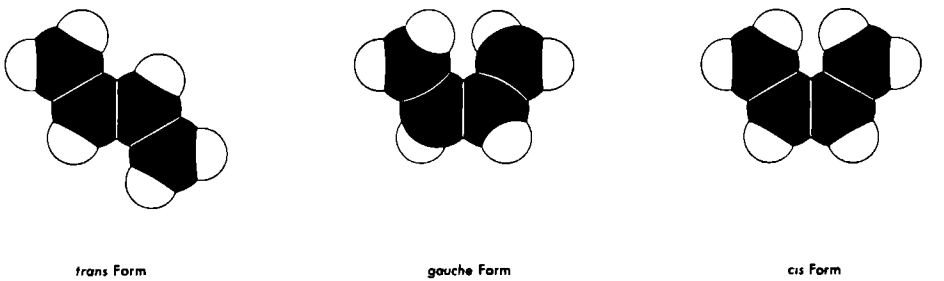

Figure 1: Structural representation of trans-, gauche- and cis 1,3-butadiene.

The Raman spectrum has been measured in 1975 and the trans cis interconversion barrier was found to be 2504 cm^{-1} [12]. Starting from a different molecular geometry the group

of Durig has reinterpreted the measurements and presented a different possible assignment. According to their trans-gauche-gauche potential a new Raman transition should be observed for the minor conformer at about 217 cm^{-1}, which would have no counterpart for a cis-geometry. As a matter of fact this transition belongs to a tunnelling doublet of a gauche level with three torsional quanta of excitation in the upper level. The corresponding gauche-gauche tunneling splitting amounts to about 40 cm^{-1} [13].

In this paper we present torsional Raman spectra measured in a very sensitive intercavity set up [14]. The significantly improved sensitivity has allowed us to observe the crucial transition at 214.9 cm^{-1}. In addition another new Raman line has been found for the trans conformer. –The Raman intensities reflect the influence of the twisting angle, ϕ, on the average polarizability of the molecule, in addition to the obvious Boltzmann factors. To reconcile our experimental results with Boltzmann prediction, this dependence on ϕ will be shown to enhance the intensities of the minor conformer with respect to the trans results considerably.

5.2 Experimental

The experimental arrangement has been already described before [14, 15, 16]. It consists of a very sensitive Raman spectrometer. An intracavity configuration allows a signal gain of about a factor 100 as compared to conventional extracavity measurements. Using the spontaneous Raman effect we employ a monochromator to obtain spectral selection; therefore we are limited in resolution. With a slitwidth of 100 μm, the resolution is 1.0 cm ^{1}, which results in an accuracy of 0.3 cm^{-1}.

The spectra have been recorded using the 488.0 nm laser radiation of an Ar-ion laser (Spectra Physics, model 2030–15S) for most of the measurements. The frequency scale of each spectrum is calibrated against the most intense plasma lines present in the discharge tube of the laser itself. The green laser line at 514.5 nm has been used also as excitation source to discriminate transitions from superimposed plasma lines. The signal collected by a cooled photomultiplier tube (RCA C31034-02) and averaged with a photon counting system (Ortec Brookdeal 5C1) is processed by an Apple IIe computer. The light which leaks through the folding mirror of the cavity was monitored during the scans and used afterwards to normalize the spectra. The intensity is estimated from the recording subtracting a smooth 'background' and integrating the area under the remaining peak (see fig. 2a). The spectra were recorded with scan velocities of 40 cm^{-1}/hour in case of strong transitions. Slower scans have been necessary to measure weak transitions, 8 cm^{-1}/hour .

A sample of 1.3 butadiene (99.8%) has been purchased from Intermar b.v. and used without further purification. The experiments have been performed at an optimum pressure of 500 Torr. After a few hours of measurements the Ar^{+} laser radiation produced a chemical deposit on the intracavity brewster window causing a decrease in laser power. The film

deposite could be removed easily with methanol. The measurements concerning the low frequency region have been difficult considering the Boltzmann factor for the high lying initial levels of the system. The presence of several plasma lines in this spectral range enhances these difficulties.

5.3 Theoretical aspects

For systems which consist of a frame and one or two methyl rotors, one can reasonably describe the kinematic part of the internal rotation by a constant F-value (inverse moment of inertia) and F', see e.g. [14, 15, 16]. This is because during the rotation of the methyl group the geometrical structure, and thus the principal moments of inertia, of the molecule hardly changes. In the case of 1,3-butadiene the molecular geometry changes drastically during the internal motion of the ethylic group. This means that the reduced moment of inertia strongly depends on ϕ, the torsional angle between the ethylic groups around the C–C bond. During our analysis we rely on the $F(\phi)$ values of Durig *et al.* [13]. Using the structure determined by Kuchitsu *et al.* [2], they derived a Fourier series representation

$$F(\phi) = F_0 + \sum_{i=1}^{5} F_i \,.\, \cos(i\phi), \tag{5.1}$$

in which $F_0 = 2.803$ cm^{-1}, $F_1 = -0.186$ cm^{-1}, $F_2 = 0.069$ cm^{-1}, $F_3 = -0.041$ cm^{-1}, $F_4 = 0.040$ cm^{-1}, $F_5 = -0.020$ cm^{-1}.

The Hamiltonian for the torsional motion is taken from L.A. Carreira [12] and written as follows:

$$H = -\frac{d}{d\phi}F(\phi)\frac{d}{d\phi} + V(\phi) \qquad \phi \in [0,\ 2\pi\rangle. \tag{5.2}$$

Carreira chooses as a first approximation

$$V(\phi) = \sum_{i=1}^{n} \frac{V_i}{2}\big(1 - \cos(i\phi)\big) \tag{5.3}$$

with $n = 3$. The potential constants V_1, V_2 and V_3 were determined from a fit to the observed torsional transitions. After this preliminary determination Carreira included V_4, V_5 and V_6 and concluded that inclusion of a small V_4 term slightly improved the fit, whereas the influence of V_5 and V_6 was negligible (see table 2).

In order to solve the Hamiltonian we approximate e.g. the first derivative of the eigenfunctions $\psi_i(\phi)$;

$$\frac{d}{d\phi}\psi_i(\phi) = \frac{1}{2h}[\psi_i(\phi + h) - \psi_i(\phi - h)] \tag{5.4}$$

Then the first part of the Hamiltonian can be written:

$$\frac{d}{d\phi}F(\phi)\frac{d}{d\phi}\psi_i(\phi) = \frac{F(\phi+h)}{4h^2}[\psi_i(\phi+2h) - \psi_i(\phi)] - \frac{F(\phi-h)}{4h^2}[\psi_i(\phi) - \psi_i(\phi-2h)] \quad (5.5)$$

The Hamiltonian matrix is symmetric and can easily be diagonalized with an IMSL subroutine. The eigenvalues are calculated for different step sizes, h. It was found that they converged rather fast, and that $h = 360^o/400$ was a suitable choice. The IMSL subroutine diagonalized a 400 $\times$ 400 matrix for different choices of V_i-values. These potential constants, V_i, with their errors were determined with the least-squares methode, as discussed in [14].

5.4 Results and discussion

5.4.1 The transitions

The low frequency Raman spectrum of 1,3-butadiene is shown in fig. 2a. All the lines assigned to torsional transitions are indicated. In the insert part of the spectrum is enlarged; the scanning time has been increased in order to get a better signal to noise ratio. To confirm whether the line assigned to the $3^+ \leftarrow 1^+$ torsional transition is not a plasma line, we recorded the spectrum not only with a different laser line but also on the anti-Stokes side. In the neighbourhood of the crucial transition $3^+ \leftarrow 1^+$, some other spectral features appear (see fig. 2a, insert). Going from left to right, the first little bump at 202 cm^{-1}, belongs to the pure rotational spectrum of N_2 (J = 26 $\leftarrow$ 24) as has been checked experimentally. At the right of the $3^+ \leftarrow 1^+$ transition a narrow plasma line is visible. The bump at its right side, at 226 cm^{-1}, belongs to a weak plasma line. Finally, the $3^- \leftarrow 1$ torsional transition is indicated in both curves.

To fit the torsional transitions in 1,3-butadiene, the F_i values were used from Durig *et al.* [13] (see table 2). They reexamined the potential function of butadiene obtained by L.A. Carreira [12]. After analyzing the torsional potential of glyoxal, the authors suggested that Carreira had exaggerated the C=C-C angle opening on going from the trans to the cis conformer. Radom and Pople [3] predicted theoretically that this angle might open by about 2.5°. Strengthened by the fact that similar results were found experimentally for glyoxal by Ramsay and Zauli [17], Durig *et al.* derived a Fourier series representation of F, using for the trans form the structure determined by Kuchitsu *et al.* [2]. In order to derive the structure for the cis form, the molecular parameters for the trans form were changed in a manner similar to what was used for glyoxal [13]. With these F_i values Durig *et al.* fit the measurements of Carreira. They show that with the limited experimental data of Carreira it is not possible to determine uniquely the potential function, but that a gauche form for the minor conformer appears certainly possible.

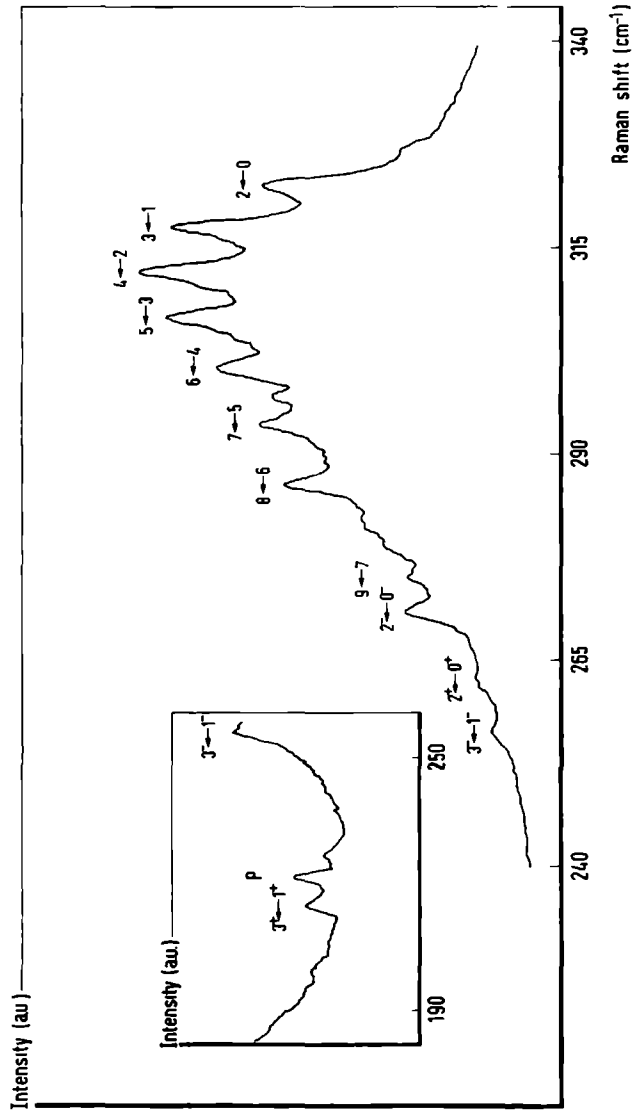
Intensity (au)
Raman shift (cm^{-1})
240
265
290
315
340
4←2
5←3
6←4
7←5
8←6
9←7
3←1
2←0
2←0
J←1
J←1
P
190
250
Intensity (au)

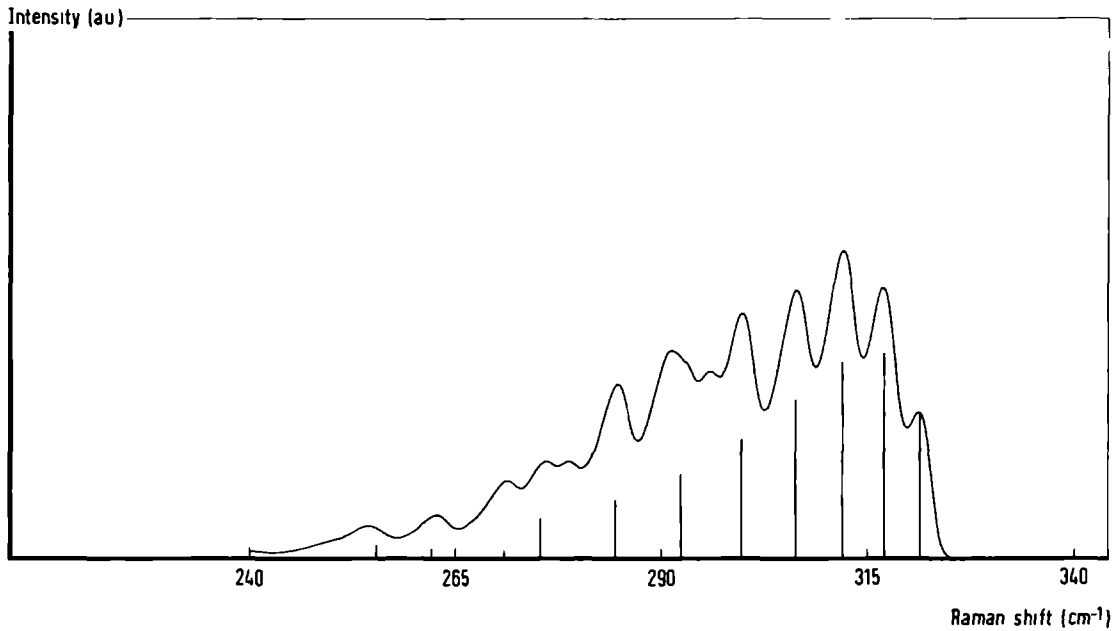

Figure 2: The measured (previous page) and calculated (this page) torsional Raman spectrum of 1,3-butadiene. The P indicates a plasma line (see also section 5.4.1).

Table 1: Observed and calculated torsional Raman transitions of 1,3-butadiene (in wavenumbers). Intensities are scaled to the intensity of the transition $3 \leftarrow 1$ and are calculated for the pure torsional transitions (see section 5.4.3).

observed		CARREIRA		DURIG		OUR RESULT		
Raman shift	intensity	assignment	calculated Raman[1] shift	assignment	calculated Raman[1] shift	assignment	calculated Raman[1] shift	calculated intensity[2]
321.6(3)	0.88	$2 \leftarrow 0$ (trans)	324.4	$2 \leftarrow 0$ (trans)	322.3	$2 \leftarrow 0$ (trans)	321.10	0.71
316.6(3)	1.00	$3 \leftarrow 1$	318.7	$3 \leftarrow 1$	318.0	$3 \leftarrow 1$	316.79	1.00
311.1(3)	0.98	$4 \leftarrow 2$	312.4	$4 \leftarrow 2$	312.9	$4 \leftarrow 2$	311.76	0.96
305.7(3)	0.77	$5 \leftarrow 3$	306.0	$5 \leftarrow 3$	307.1	$5 \leftarrow 3$	306.01	0.77
299.6(3)	0.56	$6 \leftarrow 4$	299.6	$6 \leftarrow 4$	300.6	$6 \leftarrow 4$	299.53	0.57
292.7(3)	0.49	$7 \leftarrow 5$	292.9	$7 \leftarrow 5$	293.3	$7 \leftarrow 5$	292.28	0.40
285.2(3)	0.67	$8 \leftarrow 6$	285.8	$8 \leftarrow 6$	284.9	$8 \leftarrow 6$	284.19	0.28
274.3(3)	0.19	not observed	(278)	$9 \leftarrow 7$	(274.1)	$9 \leftarrow 7$	275.17	0.19
269.9(3)	0.46	$1 \leftarrow 3$ (cis)	269.2	$2^- \leftarrow 0^-$ (gauche)	272.2	$2^- \leftarrow 0^-$ (gauche)	270.76	0.03
262.4(3)	0.09	$2 \leftarrow 4$	264.7	$2^+ \leftarrow 0^+$	263.9	$2^+ \leftarrow 0^+$	261.94	0.04
255.9(3)	0.14	$3 \leftarrow 5$	259.3(?)	$3^- \leftarrow 1^-$	256.5	$3^- \leftarrow 1^-$	255.33	0.06
214.9(3)	0.28	not observed	no assignment possible	$3^+ \leftarrow 1^+$	(217.0)	$3^+ \leftarrow 1^+$	215.02	0.17

1. calculated with the parameters given in table 2
2. assuming $\alpha_2/\alpha_1 = -0.10$, see section 5.4.2

The measured and calculated torsional Raman transitions, together with their assignment, based upon the potential constants and F_i values of table 2, are listed in table 1. In the assignment the positive or negative sign indicates the parity of the wave function belonging to the levels of the gauche conformer split due to tunnelling. In table 1, from the column with the Carreira results, it is clear that the new transition observed at 214.9 cm^{-1} can not be fitted with the Carreira potential. Durig *et al.* already mention that this transition, if measured, would strongly indicate a trans-gauche-gauche potential. With our new observations we can now state this. The torsional potential is drawn in fig. 3, using our torsional parameters.

Table 2: Torsional potential constants and F_i values of 1,3-butadiene (cm^{-1}).

	CARREIRA		DURIG		OUR RESULT	
	value	error	value	error	value	error
V_1	600	100	469.1	4.4	494.4	0.2
V_2	2068	50	1244.2	23.4	1257.1	1.4
V_3	273	8	909.0	4.9	904.8	0.7
V_4	-49	18	-177.1	7.8	-179.3	0.8
V_5					-2.3	0.4
V_6			-19.8	4.1	-20.5	0.2
F_0	3.03		2.803		2.803	
F_1	-0.687		-0.186		-0.186	
F_2	0.375		0.069		0.069	
F_3	-0.127		-0.041		-0.041	
F_4	0.039		0.040		0.040	
F_5			-0.020		-0.020	

The peak at 296.6 cm^{-1} in fig. 2a could not be assigned to a torsional transition. However, it could be a hotband transition originating from the ν_{24} CCC–deformation vibration at 301 cm^{-1} [18] and a torsional level, e.g. $\nu_{24} + (n+2).\nu_{tors} \leftarrow \nu_{24} + n.\nu_{tors}$. At room temperature 23% of the molecules are in the ν_{24} vibrational level, this means that the torsional hotband transitions should be observable with an intensity 4 times weaker than the pure torsional transitions and probably shifted. This can account for the transitions at 277 8 and 281.0 cm^{-1} which were clearly observed in a slow scan at higher resolution. A similar consideration holds for the ν_9 CCC–deformation vibration at 512 cm^{-1} [18] which is populated by 8.4 % of the molecules, at 300 K. –Part of the smooth 'background' below

the torsional transitions in fig. 2a is attributed to these hotband transitions. We tried to simulate this 'background' by adding to the calculated pure torsional spectrum the same spectrum but with the intensity of $1/4 + 1/12 = 1/3$ of the pure torsional transitions, and shifted about 15 cm^{-1} to the red (see the dashed curve in fig. 4a).

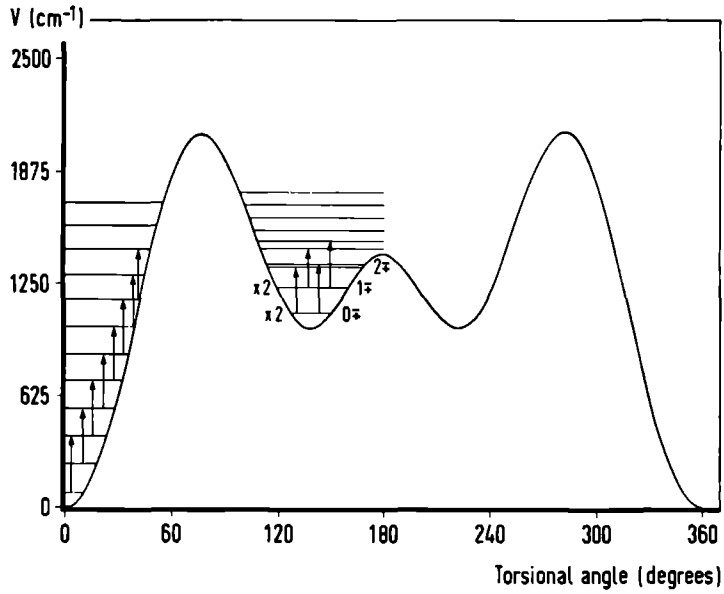

Figure 3: Torsional potential of 1,3-butadiene. The arrows indicate the transitions used to fit the potential.

5.4.2 The polarizability

The intensities of the measured transitions are determined by subtracting the smooth background from the spectrum and calculating the area under the remaining peak (see fig. 2a and table 1). Most astonishing are the intensities of the gauche compared to the trans transitions. If one assumes for the polarizability function, $\alpha(\phi)$, a $\cos(\phi)$ dependence, then the relative intensities are mainly determined by the difference in Boltzmann factors of the starting levels. At room temperature this assumption should result in a measured intensity ratio between the $2 \leftarrow 0$ 'trans' transition and the $(2^- \leftarrow 0^-)$ & $(2^+ \leftarrow 0^+)$ 'gauche'

transition of a factor 100. The fact that we find only a factor 2 & 10 led us to the conclusion that one has to include a second order term, $\cos(2\phi)$, in the Fourier expansion of the polarizability function;

$$\alpha(\phi) \propto \alpha_1 \cos(\phi) + \alpha_2 \cos(2\phi) \tag{5.6}$$

The intensities can be reproduced assuming $\alpha_2/\alpha_1 = -0.10$ (see table 1). A rather small $\cos(2\phi)$-term thus influences strongly (factor 10) the calculated intensities of the 'gauche' transitions. The only real discrepancy left is the calculated intensity compared to the measured intensity of the $2^- \leftarrow 0^-$ 'gauche' transition. However, 33 % of the measured intensity of this 'gauche' transition could originate from hotband transitions (see section 5.4.1). If the hotband transitions $\nu_{24} + 8.\nu_{\text{tors}} \leftarrow \nu_{24} + 6.\nu_{\text{tors}}$ and $\nu_9 + 8.\nu_{\text{tors}} \leftarrow \nu_9 + 6.\nu_{\text{tors}}$ are shifted 15 cm^{-1} to the red compared to the pure torsional transition, $8 \leftarrow 6$, then they appear at the same Raman shift as the $2^- \leftarrow 0^-$ transition, i.e. 269.9 cm^{-1}. Because we can assign the peaks at 296.6 cm^{-1} and at 269.9 cm^{-1} in the spectrum of fig. 2a to torsional hotband transitions, we conclude that the ν_{24} hotband torsions are indeed 15 cm^{-1} shifted to the red.

If one assumes $\alpha_2/\alpha_1 = -0.50$, a strong relative increase of the 'gauche' Raman intensities is found, too, at least for transitions starting from low torsional levels. However, the intensities of the 'trans' torsional transitions, starting from a higher level, fall off too quickly (see fig. 4b). We thus reject this possibility, also because one does not expect the second order term in the Fourier expansion (eq. (5.6)) to be so big.

5.4.3 The simulation

The simulation of the torsional spectrum of 1,3-butadiene is shown in fig. 2b. The position of the torsional transitions is calculated with the parameters of table 2. The intensities are calculated with eq. (5.6), assuming $\alpha_2/\alpha_1 = -0.10$. The sticks in figure 2b show the position and the relative intensities of the calculated pure torsional transitions. As a transition profile we choose a measured vibrational Q-branch possessing a tail to the red. The profiles are summed up to yield the pure torsional spectrum. To this spectrum is added the same spectrum, but with an intensity of 1/3 of the pure torsional spectrum, and shifted 15 cm^{-1} to the red. In figure 4 the dashed curve represents this hotband spectrum. It is clear from this figure that the hotband transitions can account for two peaks in the measured spectrum, as discussed in section 5.4.1. This simulation shows that our procedure to obtain the intensities (see section 5.4.2) is justified. To state it very clearly, there is no "background" present from other fundamentals, but the spectrum of fig. 2a results from partially overlapping torsional transitions with some hotband torsions underneath.

a)

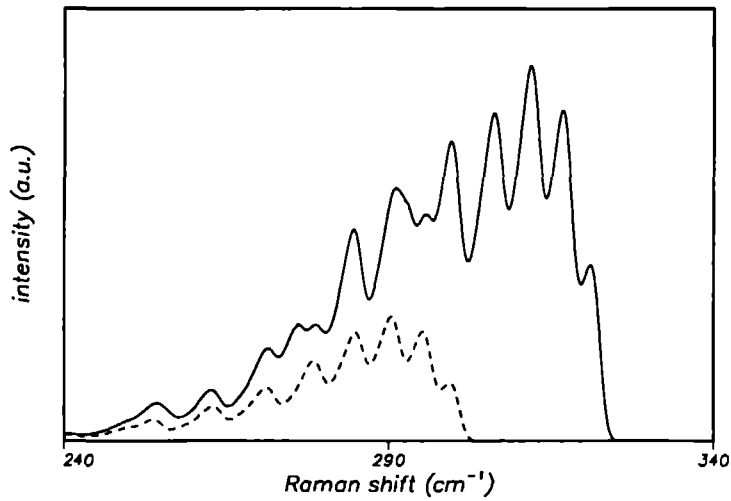

b)

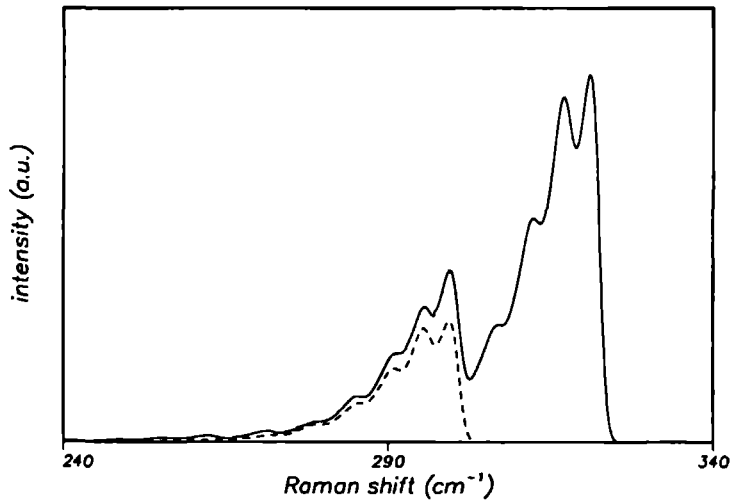

Figure 4: Calculated torsional Raman spectrum of 1,3-butadiene for $\alpha_2/\alpha_1 = -0.10$ *(a) and for* $\alpha_2/\alpha_1 = -0.50$ *(b). The dashed curve shows the torsional hotband spectrum which is added to the pure torsional Raman spectrum (see section 5.4.1)*

Acknowledgement

We thank K. J. Miller for stimulating discussions about the intensity problem, and C. Sikkens and J. Holtkamp for their technical assistance. One of us (D.C.) gratefully acknowledges the EEG for support.

References

[1] A. Almenningen and M. Traetteburg Acta Chem. Scand. **12** (1958) 1221

[2] K. Kuchitsu, T. Fukuyama and Y. Morimo, J. Mol. Struct. **1** (1968) 463

[3] L. Radom and J.A. Pople, J. Am. Chem. Soc. **92** (1970) 4786

[4] S. Skaarup, J.E. Boggs and P.N. Skancke, Tetrahedron **32** (1976) 1179

[5] J. Breulet, T.J. Lee, and H.F. Schaefer III, J. Am. Chem. Soc. **106** (1984) 6250

[6] D. Feller and E.R. Davidson, Theor. Chem. Acta **68** (1985) 57

[7] R.L. Lipnick and E.W. Garbisch Jr., J. Am. Chem. Soc. **95** (1973) 6370

[8] B.R. Arnold, V. Balaji, and J. Michl, J. Am. Chem. Soc. **112** (1990) 1808

[9] J.J. Fisher and J. Michl, J. Am. Chem. Soc. **109** (1987) 1056

[10] M.E. Squillacote, R.S. Sheridan, O.L. Chapman, and F.A.L. Anet, J. Am. Chem. Soc. **101** (1979) 3657

[11] K.B. Wiberg and R.E. Rosenberg, J. Am. Chem. Soc. **112** (1990) 1509

[12] L.A. Carreira, J. Chem. Phys. **62** (1975) 3851

[13] J.R. Durig, W.E. Bucy, and A.R.H. Cole, Can. J. Phys. **53** (1975) 1832

[14] R. Engeln, J. Reuss, D. Consalvo, J.W.I. van Bladel, A. van der Avoird and V. Pavlov-Verevkin, Chem. Phys. **144** (1990) 81

[15] R. Engeln, J. Reuss, D. Consalvo, J W.I. van Bladel and A. van der Avoird, Chem. Phys. Lett. **170** (1990) 206

[16] R. Engeln and J. Reuss, Chem. Phys., accepted for publication

[17] D.A. Ramsay and C. Zauli, Acta. Phys. Acad. Sci. Hung. **35** (1974) 79

[18] P.W. Mui and E. Grunwald, J. Am. Chem. Soc. **104** (1982) 6562

Chapter 6

The umbrella motion in ammonia

R. Engeln and J. Reuss
Department of Molecular and Laser Physics, University of Nijmegen
Toernooiveld, 6525 ED Nijmegen, The Netherlands

P. Wormer, J. van Bladel and A. van der Avoird
Theoretical Chemistry, University of Nijmegen
Toernooiveld, 6525 ED Nijmegen, The Netherlands

Abstract

The Raman spectrum of the $\nu_2(1 \leftarrow 0)$ and $\nu_2(2 \leftarrow 0)$ umbrella motion is reported. The intensities contain information about the isotropic and anisotropic part of the molecular polarizability. The aim of the investigation is to compare our experimental Raman intensities with calculated Raman ones, determined from polarizability values obtained by ab initio methodes.

6.1 Introduction

Raman spectroscopy helps to determine vibrational modes and consequently the geometrical structure, especially of molecules possessing a center-of-inversion. -Here we are interested in the information residing in the Raman-intensity, information which is related to the polarizability of the molecule.

This polarizability depends on the position of the atoms constituting the molecule. We have chosen the umbrella motion of NH_3, a motion with rather large amplitude with possibility of tunneling of the three hydrogen atoms from one side of the nitrogen atom to the other. The coordinate for this motion is the angle, ϕ, between the NH-bond and the C_3-axis (molecular z-axis). The conventional though disputable picture of hybridized sp^n-orbitals (n=2 & 3) illustrates the effect of the geometry on the polarizability. The value $\phi = 90°$ corresponds to the planar situation; here sp^2-hybridization leads to three orbitals in the x, y-plane and a single p_z-orbital perpindicular to this plane. Consequently, the two electrons in this p_z-orbital can be polarized relatively easily symmetrically along the z-axis (large α_{zz}-value) and the 6 electrons (shared by the H-atoms and the N-atom) can move rather free in the x, y-plane (large α_{xx}- and α_{yy}-values).

On the other hand, in the equilibrium position of ammonia, $\phi = 112.5°$, the sp^3-hybridization prevails, restricting the mobility of the two paired electrons mainly to one side (e.g. $z > 0$); simultaneously, the 6 shared electrons are confined in their mobility to three CH_4-like lobes, thus yielding relatively smaller values of α_{zz} and α_{xx} & α_{yy}, respectively.

Qualitatively, this behaviour is borne out by an ab initio calculation which is reported in section 6.3. The aim of this investigation is to compare quantitatively experimental results of Raman-intensities with polarizability-values (as function of ϕ) obtained by ab initio methodes.

6.2 Experimental

The setup is described in chapter 1 of this thesis. The spectra have been recorded using the 514 5 nm laser radiation of the Ar-ion laser (Spectra Physics, model 2030–15S) for all the measurements.

During the experiments the pressure of the ammonia was 600 Torr. Due to the contamination of the brewster window of the cell by the ammonia, the laser power could only be kept constant for about one hour. This is the reason why most of the spectra shown here have a rather poor signal to noise ratio. The spectra for the total intensity were recorded with scan velocities of 360 cm^{-1}/hour. Because we wanted to measure the parallel and the perpendicular part (with respect to the laser polarization) of the molecular polarizability, α, separately, we inserted a polaroid and a scrambler between the cell and the entrance slit of the monochromator. Both polaroid and scrambler introduce extra losses in the transmitted

Raman-light, which forced us to make slower scans, 150 cm ^{1}/hour . The polaroid is used to select one component ($\perp$ or $\parallel$) of the scattered light, and the scrambler is used to convert it into randomly polarized light. In this way one does not have to correct for the polarization dependence of the reflectivity of the gratings, i.e. the intensities of both spectra ($\perp$ and $\parallel$) can be compared without any scaling.

6.3 Theoretical aspects

In the case of spontaneous Raman scattering, the induced electric dipole moment, $\bar{P}$, is given by

$$\bar{P} = \boldsymbol{\alpha}.\bar{E}, \tag{6.1}$$

in which $\boldsymbol{\alpha}$ is the polarizability tensor, possessing nine coefficients, α_{ij} $(i, j = x, y, z)$. Since in the experiment the frequency of the incident light is far off a rovibronic resonance, we only need to consider a real symmetric polarizability tensor. The consequences are that $\alpha_{xy} = \alpha_{yx}$, $\alpha_{xz} = \alpha_{zx}$ and $\alpha_{zy} = \alpha_{yz}$ and that the tensor has a maximum of six distinct real components.

On rotation of the axis system, the values of individual components of the polarizability tensor change. However, certain combinations remain invariant. For the real symmetric polarizability tensor they are the isotropic polarizability, $\overline{\alpha}$, defined by

$$\overline{\alpha} = \frac{1}{3}(\alpha_{xx} + \alpha_{yy} + \alpha_{zz}) \tag{6.2}$$

and the anisotropy, γ, defined by

$$\gamma^2 = \frac{1}{2}\big((\alpha_{xx} - \alpha_{yy})^2 + (\alpha_{yy} - \alpha_{zz})^2 + (\alpha_{zz} - \alpha_{xx})^2 + 6(\alpha_{xy}^2 + \alpha_{yz}^2 + \alpha_{zx}^2)\big) \tag{6.3}$$

Because of its geometry we can write for ammonia

$$\overline{\alpha} = \frac{1}{3}(2\alpha_{xx} + \alpha_{zz}) \tag{6.4}$$

and

$$|\gamma| = |\alpha_{xx} - \alpha_{zz}|. \tag{6.5}$$

On page CRS 16 in [2] the general forms for $I_\perp$ and $I_\parallel$ are given for an observation geometry as we have applied, in which the scattered light is observed under 90^o with respect to the propagation and polarization of the incident light. For $\Delta\nu = +1$ is found

	$I_\parallel$	$I_\perp$
$\Delta J = 0$	$(\overline{\alpha}')^2 + \frac{4}{45}C(\gamma')^2$	$\frac{1}{15}C(\gamma')^2$
$\Delta J \neq 0$	$\frac{4}{45}C(\gamma')^2$	$\frac{1}{15}C(\gamma')^2$

where C is responsible for the relative anisotropic intensities of individual rotational lines. The formulaes can be applied also to $\Delta\nu = +2$ transitions; $\overline{\alpha}'$ and γ' have to be replaced by $\overline{\alpha}''$ and γ'', respectively.

a)

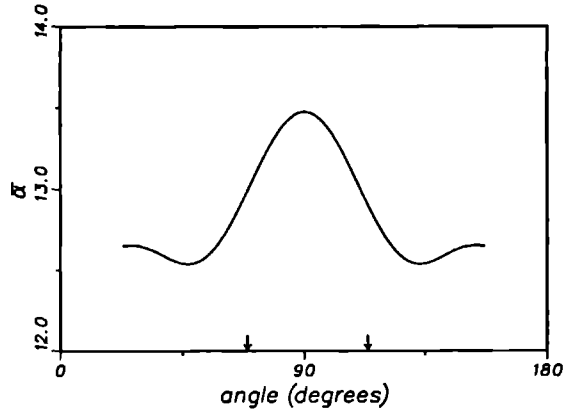

b)

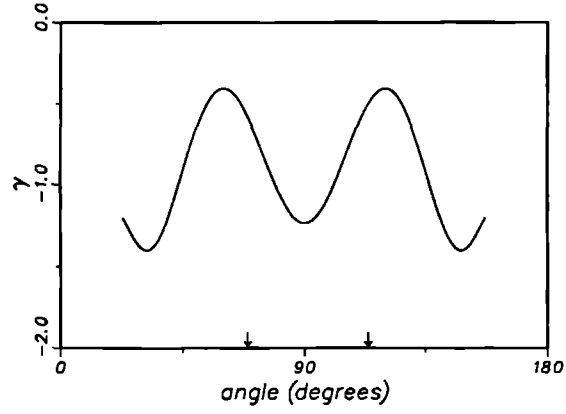

Figure 1: Calculated $\overline{\alpha}$ (a) and γ (b) of ammonia. The wavefunctions vanish at the boundaries of both curves, $\phi = 157\ 5°$ and $\phi = 22.5°$. The arrows indicate ϕ in the equilibrium geometry.

6.4 Results and discussion

6.4.1 the $\nu_2\,(1 \leftarrow 0)$ transition

a)

b)

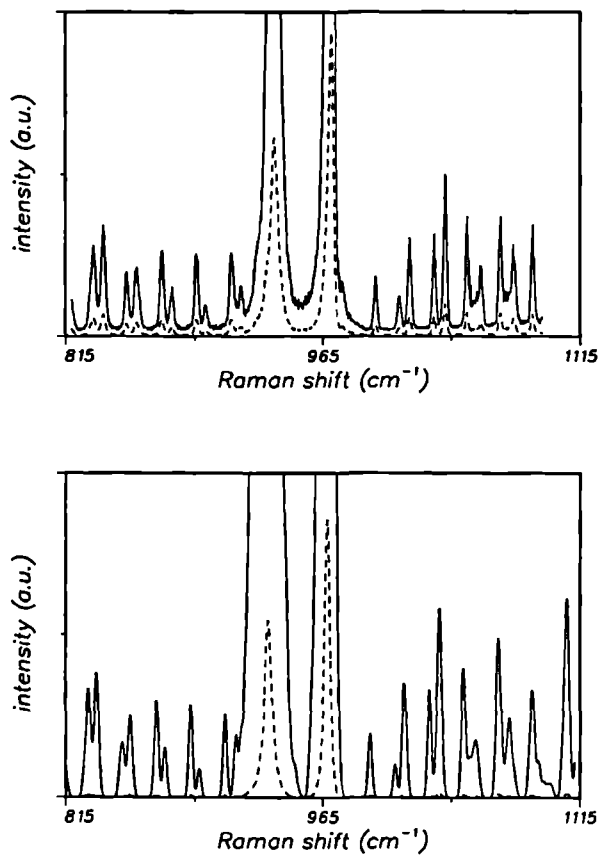

Figure 2: Measured (a) and calculated (b) $\nu_2(1 \leftarrow 0)$ Raman spectrum of ammonia. The spectrum indicated by the solid line is enlarged by a factor of 5 in 'a', and 50 in 'b'

In figure 2a part of the ν_2 Raman spectrum of $^{14}NH_3$ is shown. This spectrum is recorded without the use of a scrambler or polaroid, i.e. the total intensity, I_{tot}, is measured (a small error is made if one compares the calculated and measured I_{tot}, because the measured I_{tot} is not just $I_\perp + I_\parallel$). Clearly observable are two Q-branches with O-, P-, R- and S-branches. The two Q-branches are separated by the inversion splitting of the first excited

ν_2-state, which amounts to about 34.9 cm^{-1}; the splitting in the ground state is about 0.79 cm^{-1} [1]. We will denote the branches with a '+' and a '−', depending on the symmetry of the wavefunction with respect to inversion; '+' means symmetric, '−' means anti-symmetric. To every Q-branch belongs a O-, P-, R- and S-branch. The ground-state and ν_2-excited state molecular parameters of $^{14}NH_3$ are very well known [1] (see table 1). Using the molecular

Table 1: Ground-state, ν_2-state and $2\nu_2$-state molecular parameters of $^{14}NH_3$ (in cm^{-1}).

	ground-state a)	ν_2-state a)	$2\nu_2$-state
ν_0^+ [d]	0.0	932.43384	1597.4697[b]
B^+	9.94664	10.07018	10.19376[c]
C^+	6.22836	6.08917	5.94998[c]
ν_0^- [e]	0.79341	967.32854	1881.3817[b]
B^-	9.94158	9.89003	9.83845[c]
C^-	6.23531	6.34084	6.44627[c]

a) from [1]
b) from [3]
c) our extrapolated values
d) defined as $(E_r^+ - E_n^+)/hc$
e) defined as $(E_r^- - E_n^-)/hc$

parameters from [1], we can reproduce the measured transition frequencies (see table 2).

As can be seen from figure 2a and 2b, the relative intensities of the two Q-branches and the relative intensities within and between the O-, P-, R- and S-branches reproduce the calculated intensities fairly well. However, there is a big discrepancy between the calculated and measured ratio of the Q-branch intensity to the O-branch intensity; the calculated $I_{tot}(Q)/I_{tot}(O)$ is about 10 times bigger than the measured ratio.

Several transitions have been measured using a scrambler and a polaroid in order to measure separately $I_\perp$ and $I_\parallel$. The results for the Q-branches are shown in figure 3. The calculations for the O-, P-, R- and S-branches are in good agreement with the measurements. The calculated $I_\parallel / I_\perp$ for the Q-branches is about a factor of 10 bigger than the measured ratio (see fig. 3), which is consistent with the factor of 10 in the I_{tot} ratio. With the help of the formulaes in section 6.2 one can show that $(\alpha'/\gamma')^2_{exp} = \frac{1}{10}\,(\overline{\alpha}'/\gamma')^2_{calc}$. From the ab initio calculation follows that for the equilibrium geometry, $\phi = 112.5°$, $(\overline{\alpha}'/\gamma')^2 = 1.1560$ (assuming a harmonic approximation). To be more accurate, one should take the sandwich

integral of $\bar{\alpha}'$ and γ' with the ground- and first excited ν_2-state wavefunctions, instead of α' and γ'.

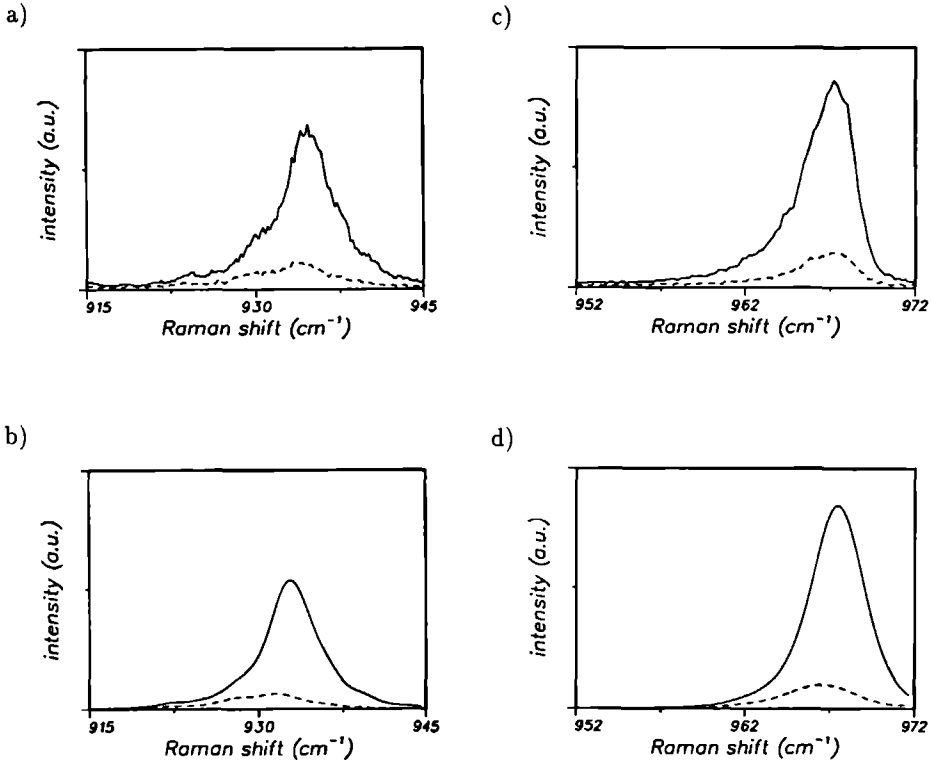

Figure 3: Measured (a,c) and calculated (b,d) Q^+- and Q^--branches of the $\nu_2(1 \leftarrow 0)$ transition of ammonia. The intensities in the calculated and measured spectra are scaled to the intensity of the Q^--peaks. The solid (dashed) curves indicate $I_{\parallel}$ ($I_{\perp}$). The calculated $I_{\perp}$ curves are enlarged by a factor of 10. See also section 6.4.1.

6.4.2 the $\nu_2\,(2 \leftarrow 0)$ transition

In figure 4a part of the measured $\nu_2\,(2 \leftarrow 0)$ Raman spectrum of ammonia is shown. As in the previous case, one expects two Q-branches and two sets of O-, P-, R- and S-branches. The inversion splitting in the second excited ν_2-state is experimentally determined to be 284 cm^{-1} [3]. The Q^+-branch should be found at a Raman shift of about 1598 cm^{-1};

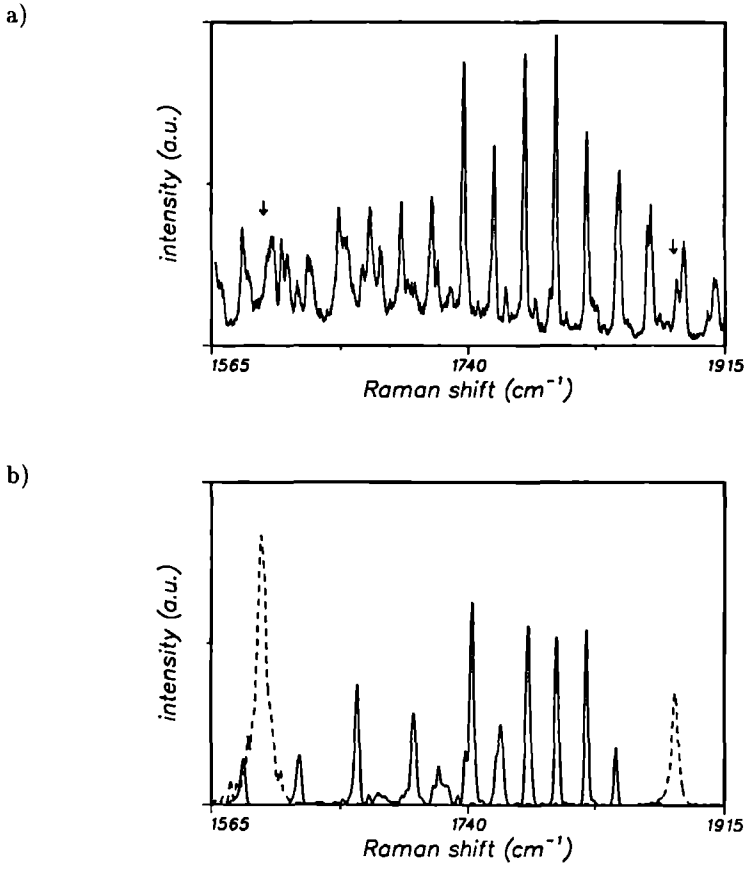

Figure 4: Measured (a) and calculated (b) $\nu_2(2 \leftarrow 0)$ Raman spectrum of ammonia. In (b) the spectrum indicated by the solid line is enlarged by a factor of 100 and the Q-branch transitions are left out.

the Q^--branch at about 1882 cm^{-1}. The calculation yields two strong Q-branches. In the measured spectrum no clear Q-branch is visible, but we tentatively assign the two features marked with an arrow to the Q-branches (see fig. 4a). In figure 4b the calculated spectrum is shown. The 'dashed' spectrum shows only the calculated Q-branch transitions. The spectrum indicated by the solid line, is enlarged by a factor of 100 and shows only the O-, P-, R- and S-branches. Again, the relative intensities within the O-, P-, R- and S-branches agree well with the calculated values. However, in this case the calculated $I_{tot}(Q^+)/I_{tot}(O^-)$ is

about a factor 450 bigger than measured. This means that $(\overline{\alpha}''/\gamma'')^2_{\mathrm{exp}} = \frac{1}{450}\,(\overline{\alpha}''/\gamma'')^2_{\mathrm{calc}}$. As in section 6.4.1, one calculates $(\overline{\alpha}''/\gamma'')^2 = 0.0205$, at $\phi = 112.5^o$. The same remark has to be made as in section 6.4.1; one should take the sandwich integral of $\overline{\alpha}''$ and γ'' with the ground- and the second excited ν_2-state wavefunctions, instead of $\overline{\alpha}''$ and γ''.

The calculation shows that most of the intense features can be assigned to O^- and P^- transitions (see table 2), and that the smaller peaks in between are S^+ and R^+ transitions.

In order to calculate the $\nu_2\,(2 \leftarrow 0)$ transition frequencies we had to know the rotational constants for the $2\nu_2$. We used a linear extrapolation of the rotational constants of the ground-state and the first excited ν_2 state [1]. The band origin was taken from [3] (see table 1).

Acknowledgement

We like to thank Edgar Olthof for some calculations on the energy levels.

References

[1] Š. Urban, V. Špirko, D. Papoušek, J. Kauppinen, S.P. Belov, L.I. Gershtein, A.F. Krupnov, J. Mol. Spectrosc. **88** (1981) 274

[2] D.A. Long, *Raman Spectroscopy*, McGraw-Hill, London (1977)

[3] Š. Urban, V. Špirko, D. Papoušek, R.S. McDowell, N.G. Nereson, S.P. Belov, L.I. Gershtein, A.V. Maslovsky, A.F. Krupnov, J.B. Curtis, and K.Narahari Rao, J. Mol. Spectrosc. **79** (1980) 455

Table 2: Observed and calculated Raman transitions, $\nu_2(1 \leftarrow 0)$ and $\nu_2(2 \leftarrow 0)$, of ammonia (in cm^{-1}).

observed Raman shift	assignment[a] $\nu_2(1 \leftarrow 0)$	calculated Raman[b] shift	observed Raman shift	assignment[a] $\nu_2(2 \leftarrow 0)$	calculated Raman[b] shift
826.9(5)	$6^- \leftarrow 7^-$	827.43	1572(2)	$8^- \leftarrow 6^-$	1586.5
	$2^- \leftarrow 4^-$		1588(1)	?	
832.5(5)	$4^+ \leftarrow 5^+$	833.82	1607(2)	$Q^+(?)$	1598.9
	$1^+ \leftarrow 3^+$		1615(1)	$5^- \leftarrow 7^-$	1624.2
845.9(5)	$5^- \leftarrow 6^-$	847.12	1618(1)	?	
851.8(5)	$3^+ \leftarrow 4^+$	852.41	1626(1)	?	
867.9(5)	$4^- \leftarrow 5^-$	867.75	1633(2)	?	
	$1 \leftarrow 3^-$		1653(1)	$4^- \leftarrow 6$	1664.7
873.7(5)	$2^+ \leftarrow 3^+$	872.62	1667(1)	?	
886.4(5)	$3 \leftarrow 4^-$	887.53	1673(1)	?	
891.8(5)	$1^+ \leftarrow 2^+$	892.62	1680(1)	?	
906.8(5)	$2 \leftarrow 3^-$	907.63	1693(1)	$3^- \leftarrow 5^-$	1702.8
	$0^- \leftarrow 2^-$		1714(1)	$7^- \leftarrow 8^-$	1725.0
912.4(5)	$12^\tau \leftarrow 12^+$[c]	913.88	1736.8(5)	$6 \leftarrow 7^-$	1737.8
932.1(5)	$\Delta J^+ = 0$	932.85		$2^- \leftarrow 4^-$	1742.3
965.7(5)	$\Delta J^- = 0$	967.66	1757.9(5)	$5^- \leftarrow 6^-$	1762.0
991.7(5)	$3^- \leftarrow 2^+$	993.3	1779.3(5)	$1^- \leftarrow 3^-$	1781.9
1005(1)	$2^- \leftarrow 1^-$	1007.0		$4^- \leftarrow 5^-$	
1011.4(5)	$4^+ \leftarrow 3^+$	1011.9	1800.5(5)	$3^- \leftarrow 4^-$	1801.0
1025.9(5)	$3^- \leftarrow 2^-$	1026.2	1821.6(5)	$0^- \leftarrow 2^-$	1821.7
	$2^- \leftarrow 0^-$			$2^- \leftarrow 3^-$	
1032.4(5)	$5^+ \leftarrow 4^-$	1031.9	1843.6(5)	$1^- \leftarrow 2^-$	1841.6
	$3^+ \leftarrow 1^-$		1862.6(5)	?	
1044.8(5)	$4^- \leftarrow 3^-$	1045.1	1865.0(5)	?	
1052(1)	$6^+ \leftarrow 5^+$	1053.3	1882.2(5)	$Q^-(?)$	
1064.2(5)	$5^- \leftarrow 4^-$	1067.5	1887.0(5)	?	
	$3^- \leftarrow 1^-$		1908.1(5)	?	
1072(1)	$4^+ \leftarrow 2^+$	1075.3			
1083.2(5)	$6^- \leftarrow 5^-$	1086.8			

a. $J' \leftarrow J''$, $\Delta K - 0$

b. calculated with the parameters given in table 1

c. $\Delta K = 0$, $|K| = 12$

Samenvatting

Raman spectroscopie aan moleculen met interne vrijheidsgraden

De resultaten die weergegeven zijn in dit proefschrift, zijn behaald met een intracavity Raman opstelling. De opstelling bestaat uit een Ar-ion laser, waarvan de uitkoppelspiegel is vervangen door twee gekromde spiegels die zó geplaatst zijn dat er een scherp focus onstaat in de lasercavity. Op deze manier kan het gas dat bestudeerd wordt in de cavity geplaatst worden, zodat er optimaal gebruik gemaakt wordt van het aanwezige laservermogen.

Tijdens het experiment wordt laserlicht verstrooid aan moleculen in de gasfase. De moleculen die meedoen aan het Raman proces worden geëxciteerd naar een virtuele (zeer kort levende) toestand, waarna ze terugvallen naar een rotationeel of vibrationeel aangeslagen toestand onder uitzenden van een foton. Als het molecuul na het verstrooiings proces zich in dezelfde toestand bevindt als ervoor, noemt men het Rayleigh verstrooiing (het verstrooide licht heeft dezelfde frequentie als het laserlicht). Raman (anti-)Stokes verstrooiing is het proces waarbij het molecuul na excitatie meer (minder) energie bevat dan ervoor (het verstrooide licht is rood (blauw) verschoven t.o.v. het laserlicht). Het verstrooide licht wordt gedispergeerd door een dubbele monochromator, en vervolgens gedetecteerd met een photomultiplier buis. De resolutie van de gemeten spectra wordt bepaald door de eigenschappen van de monochromator, en is typisch 1.0 à 2.0 cm^{-1}.

In het proefschrift worden moleculen beschreven die bewegingen kunnen uitvoeren terwijl een deel van het molecuul -het frame- in rust blijft. Bij propaan (hoofdstuk 1) en dimethylamine (hoofdstuk 2) bestaat het frame uit een CH_2, respectievelijk, NH-groep. Aan het frame zijn twee methyl-groepen gebonden met een enkele binding. Beide methyl-groepen kunnen rond deze binding een meer vibrationele dan wel meer rotationele beweging uitvoeren. Voor welke beweging het molecuul kiest hangt af van de hoeveelheid energie die in het molecuul aanwezig is.

De CH_3-groep zal bij een volledige rotatie over 360^o , 3 maal gehinderd worden door een potentiaal barrière van het frame. Als de hoeveelheid energie niet groot genoeg is om de barrière te overbruggen, zal de CH_3-groep een vibrationele beweging uitvoeren rond het minimum. Naarmate de hoeveelheid energie groter wordt zal de beweging steeds meer gaan lijken op een vrije rotatie. Klassiek ligt het omslagpunt rotatie/vibratie bij de top van de potentiaal barrière. Quantum mechanisch is het mogelijk om door de barrière heen te tunnelen, zodat er een geleidelijke overgang ontstaat van vibratie naar 'vrije' rotatie.

Er is veel aandacht besteed aan de bepaling van de constanten die de potentiaal barrière beschrijven. De potentiaal beschrijft niet alleen de interactie tussen het frame en de top, maar ook de interactie tussen de twee toppen onderling.

In hoofdstuk 4 zijn moleculen beschreven die het etheen molecuul als basis hebben. Propeen wordt gevormd door in etheen één waterstof atoom te vervangen door één CH_3-groep. Trans-, cis- en isobuteen worden gevormd door twee waterstof atomen te vervangen door een CH_3-groep. Er is vooral gekeken naar de invloed van de relatieve posities van de CH_3-groepen op de hoogte van de potentiaal barrière.

In hoofdstuk 5 is een molecuul bestudeerd dat bij interne rotatie van structuur verandert. Beide structuren hebben niet dezelfde nulpuntsenergie en het molecuul moet om van de ene structuur naar de andere over te gaan een barrière overkomen. Door niet alleen naar de positie maar ook naar de intensiteit van de overgangen te kijken, is het gelukt om de structuur, horende bij het tweede (hoger gelegen) minimum, eenduidig te bepalen.

Naast deze wel afgeronde onderzoekingen vindt men in dit proefschrift (in de inleiding en hoofdstuk 6) twee voorlopige resultaten, te weten het Raman spectrum van de torsie beweging van tri-methylamine en een beschouwing van de Raman-intensiteiten by $\Delta\nu = 1$ & $\Delta\nu = 2$ overgangen van ammonia (excitatie van de umbrella-mode ν_2). Met name deze NH_3-resultaten leveren ondanks hun voorlopig karakter heel verrassende berekende intensiteiten op

Curriculum Vitae

Richard Antonius Hendricus Engeln

Geboren:	13 februari 1964
Geboorteplaats	Geleen
1976–1982	gymnasium B, scholengemeenschap St.Michiel te Geleen
1982–1987	studie natuurkunde aan de Katholieke Universiteit Nijmegen; afgestudeerd bij de experimentele afdeling Molekuul- en Laserfysika van Prof.dr. J. Reuss
1986	student-assistent bij het praktikum voor 2^{de}-jaars natuurkunde studenten
1986–1987	dubbel-resonantie experiment aan C_2H_4 in een molekulaire jet m.b.v. een CO_2- en FCL-laser (afstudeerproject)
1987–1991	promotie-onderzoek op de afdeling Molekuul- en Laserfysika met Prof.dr. J. Reuss als promotor. Resultaten van het onderzoek zijn weergegeven in dit proefschrift. In het kader van de onderwijsbegeleiding werd er de laatste twee jaar assistentie verleend bij het praktikum voor natuurkunde- en scheikunde studenten
maart 1988–mei 1988	bij het onderzoekscentrum ENEA, Frascati (Italië) een experimentele opstelling gebouwd waarmee m.b.v. coherente anti-Stokes Raman scattering (CARS) laser geïnduceerde processen bestudeerd kunnen worden
oktober 1989	CARS-opstelling van ENEA gebruikt om het foto-dissociatie proces van benzeen en chloro-benzeen te bestuderen.
september 1991	BOXCARS-opstelling in het combustion center van Lund (Zweden) gebruikt om het torsiespectrum van propaan, met een resolutie van 0.1 cm^{-1}, te meten

Publications

Ethylene hot bands from molecular jet double-resonance spectroscopy
N. Dam, R. Engeln, J. Reuss, A.S. Pine and A. Fayt
Journal of Molecular Spectroscopy **139** (1990) 215

Internal motion of two-top molecules: propane and dimethylamine
R. Engeln, J. Reuss, D. Consalvo, J.W.I. van Bladel and A. van der Avoird
Chemical Physics Letters **170** (1990) 206

Torsional motion of the CH_3 groups of propane studied by Raman overtone spectroscopy
R. Engeln, J. Reuss, D. Consalvo, J.W.I. van Bladel, A. van der Avoird and V. Pavlov-Verevkin
Chemical Physics **144** (1990) 81

Coherent anti-Stokes Raman scattering instrument for diagnostics of laser induced processes
R. Engeln, R. Fantoni and G. Schina
Il Nuovo Cimento **12D** (1990) 209

Raman study of the internal motion of two-top molecules: propane and dimethylamine
R. Engeln, D. Consalvo, J. Reuss, J.W.I. van Bladel and A. van der Avoird
Proceedings of the Twelfth International Conference on Raman Spectroscopy,
John Wiley & Sons (1990)

Optical detection of benzene fragmentation in I.R. and vis.-u.v. laser induced processes
R. Engeln and R. Fantoni
Il Nuovo Cimento **D**, accepted for publication

Methylic Torsion in $C_2H_{4-n}(CH_3)_n$, n=1 & 2
R. Engeln and J. Reuss
Chemical Physics, accepted for publication

Evidence for a minor gauche-conformer of 1,3-butadiene
R. Engeln, D. Consalvo and J. Reuss
submitted to Chemical Physics